Technological University Dublin
ARROW@TU Dublin

Masters | Science

2001

Design, Construction and Testing of a Portable Electronic Speckle Pattern Interferometry System for Contouring Applications

Tara J. Kneafsey
Technological University Dublin

Follow this and additional works at: https://arrow.tudublin.ie/scienmas

Part of the Physical Sciences and Mathematics Commons

Recommended Citation

Kneafsey, T.J. (2001). Design, Construction and Testing of a Portable Electronic Speckle Pattern Interferometry System for Contouring Applications. Masters dissertation. Technological University Dublin. doi:10.21427/D7761T

This Article is brought to you for free and open access by the Science at ARROW@TU Dublin. It has been accepted for inclusion in Masters by an authorized administrator of ARROW@TU Dublin. For more information, please contact arrow.admin@tudublin.ie, aisling.coyne@tudublin.ie, vera.kilshaw@tudublin.ie.

DESIGN, CONSTRUCTION AND TESTING OF A PORTABLE ELECTRONIC SPECKLE PATTERN INTERFEROMETRY SYSTEM FOR CONTOURING APPLICATIONS.

by

Tara J. Kneafsey B.Sc. (App. Sc.)

A thesis submitted for the degree of Master of Philosophy to the School of Physics

Dublin Institute of Technology

Supervised by Dr. Vincent Toal

August 2001

Declaration of Originality

I certify that this thesis which I now submit for examination for the award of Master of Philosophy is entirely my own work and has not been taken from the work of others save and to the extent that such work has been cited and acknowledged within the text of my work.

This thesis was prepared according to the regulations for postgraduate studies by research of the Dublin Institute of Technology and has not been submitted in whole or in part for an award in any other Institute or University.

The Institute has permission to keep, to lend or to copy this thesis in whole or in part, on condition that any such use of the material of the thesis be duly acknowledged.

Signature: Tara Kneafsey Date: 22-08-2007

Tara J. Kneafsey

Acknowledgements

During the time it took for me to complete this thesis, many people gave me advice, encouragement and support on many levels. First and foremost I wish to thank my supervisor Dr. Vincent Toal, for his constant support and help, but especially for never being too busy for my many queries.

I would also like to thank my research colleagues in the Centre for Industrial and Engineering Optics. For extensive help with my experimental technique, I would like to single out Dr. Brian Bowe. For support, encouragement, brain-storming sessions and an occasional shoulder to cry on, I am forever indebted to Dr. Suzanne Martin for what must add up to hours and hours of her time.

I'd also like to thank the staff of the School of Physics, but in particular Mr. Joe Keogh for his help with the miniature rotation stage electronics among other things. Special thanks also to Mr. James Callis and Mr. Enda O'Flaherty. I also wish to thank my fellow postgraduate students, for many enlightened conversations about everything but physics over the last two years!

I am indebted also to my friends who have listened without complaint to however I felt about my thesis from day to day. In particular, Clodagh and Karen and--I literally would not have survived without your input both technical and personal!

Special thanks to Leo, Lorraine and Robert for the roof over my head that has made this experience more financially viable and for the family atmosphere which has been a support through the years.

Thanks to Kevin and Letty for all the years of support and encouragement. Thanks to Clodagh Daly for the final proof-read-I'll return the favour some day! And to the best friend and proofreader one could ever wish for----thank-you Ro.

Finally, I'd like to thank my family for their unconditional support and love throughout my entire educational career -Mum and Dad, Gene, Gary and Donna and Margaret.

"Though I did not have my mother long, she cast over me an influence that has lasted all my life. My mother was the making of me"

Thomas A. Edison

Design, Construction and Testing of a portable ESPI contouring System.

Tara Kneafsey

Abstract

Optical surface metrology techniques offer many advantages over conventional methods. Some of these advantages include a greater sensitivity and a whole-field analysis that is non-contact. They also offer greater lateral and vertical resolution and are not subject to electromagnetic influence. Despite these many advantages, there has been reluctance in industry to adopt these techniques. This reluctance can be attributed to the use of high-power lasers which are considered dangerous, the expense of the systems and complicated operation and analysis procedures. The objective of the research described in this thesis was to utilise recent developments in laser diodes, data acquisition techniques and software to develop a portable miniature system suitable for industrial use.

The system described here has utilised different aspects of ESPI contouring design in the past, to produce a system, which has been optimised for industrial use. The system is stable, portable and robust. The software used was designed to be user friendly and to allow for efficient data analysis.

The system is capable of producing fringe patterns that represent the surface contour of an object under examination. It incorporates frequency modulation phase shifting for the purposes of analysis. The system has been tested extensively with satisfactory results. Proposals for improvements and further work have been made in the conclusion of the thesis.

Summary

This thesis is the result of extensive work in the area of Electronic Speckle Pattern Interferometry (ESPI), particularly ESPI contouring or profilometry. It describes the design, construction and subsequent testing of a portable and miniature ESPI contouring system.

Chapter 1 introduces ESPI in the context of Optical Metrology and Non-Destructive Testing. This chapter also outlines the research objectives of the project.

Chapter 2 describes in detail the theory behind the speckle phenomenon and Speckle Correlation Interferometry. It outlines the different types of ESPI systems and their different optical configurations. The chapter includes the theory of ESPI contouring systems. The section also deals with fringe analysis and discusses some of the many methods that are utilised in this field today. It describes fringe counting as a method of analysis along with the phase analysis technique used in this thesis.

Chapter 3 describes the experimental work carried out during the course of the research. This includes work carried out in the European Commission Joint Research Centre, Ispra, Italy on spectral contouring. It also describes bench prototypes of the final miniature system, which were built in the early stages of the research. Finally it describes the design considerations, equipment selection and final construction of the portable system.

Chapter 4 contains the results obtained by fringe counting analysis on two simple shapes, showing the system to be working effectively.
Chapter 5 contains the results obtained by phase shift analysis on two different shapes.

Chapter 6 concludes the thesis by outlining the progress made, problems faced and dealt with, suggested improvements and further work

Each chapter is referenced liberally for the reader's convenience. Overall the thesis presents an ESPI contouring system with analysed results in detail showing the system to be effective as a whole-field profilometer.

Relevant Publications and Presentations:

Conference Proceedings:

1. T. Kneafsey, V. Toal, B. Bowe. "*Shape Measurement by Electronic Speckle Pattern Interferometric Contouring.*" Meeting on Optical Techniques for Shape Measurement, Institute of Physics, 76, Portland Place, London. 27th October 1999.

Poster Presentations:

1. T. Kneafsey, V. Toal, B. Bowe " *Design, Construction and Testing of Portable Optical Metrology Systems*" Dublin Institute of Technology, Postgraduate Open Day March 1999.

2. T. Kneafsey, V. Toal, B. Bowe " *Design, Construction and Testing of an ESPI Contouring system*" 51st Irish Universities Chemistry Colloquium, Dublin, 23rd-25th June, 1999.

Table of Contents

CHAPTER 1.0 INTRODUCTION **1**

1.1OPTICAL METROLOGY 1
1.2 NON-DESTRUCTIVE TESTING (NDT) 2
1.2.1 Introduction 2
1.2.2 Non optical techniques 3
1.2.2.1 Acoustic Emission 3
1.2.2.2 X-ray scanning 4
1.2.2.3 Ultrasound 4
1.2.2.4 Elcctrical Transducers 5
1.2.3 Optical Techniques 6
1.2.3.1 Holographic Interferometry 6
1.2.3.2 Moiré Methods 7
1.2.3.3 Speckle Techniques 8
1.3 SURFACE PROFILING 11
1.3.1 Introduction 11
1.3.2 Non-Optical methods for profiling 12
1.3.2.1 Stylus Profilometry 12
1.3.3 Optical Techniques 13
1.3.3.1 Introduction 13
1.3.3.2 Low-coherence profiling techniques 14
1.3.3.3 Speckle Profiling Techniques 14
1.4 RESEARCH OBJECTIVE 16
1.5 REFERENCES 18

CHAPTER 2.0 SPECKLE TECHNIQUES AND ANALYSIS ***20***

2.1 THE SPECKLE EFFECT 20
2.2 SPECKLE PHOTOGRAPHY 26
2.3 SPECKLE PATTERN CORRELATION INTERFEROMETRY 28

2.3.1Basic Principles of Interferometry 28
2.3.2 Electronic Speckle Pattern Interferometry (ESPI) 31
2.4 ESPI SYSTEMS 32
2.4.1 In-Plane ESPI 33
2.4.2 Out of Plane ESPI. 35
2.4.3 Shearing ESPI (Shearography) 38
2.4.4 ESPI Contouring (Profilometry) 41
2.5 FRINGE ANALYSIS 44
2.5.1 Introduction 44
2.5.2. Intensity based techniques 44
2.5.2.1 Fringe Counting 45
2.5.2.2. Automatic fringe location 48
2.5.3 Phase-Shifting 50
2.5.4 Phase Unwrapping 53
2.6 REFERENCES 58

CHAPTER 3.0 SYSTEM DESIGN ***60***

3.1 LITERATURE REVIEW 60
3.2 CONTOURING TECHNIQUES 60
3.2.1 Spectral Contouring 61
3.2.2 Angle of illumination change 62
3.3 BENCH PROTOTYPES 63
3.3.1 Spectral Contouring- 64
3.3.2 Angle of Illumination change 66
3.4 MINIATURE ROTATION STAGES 67
3.4.1 LabVIEW(c) software 68
3.5 BUILDING THE SYSTEM 69
3.5.1 System layout 69
3.5.2 ESPITest software 73
3.6 COMPARISON OF THE TWO METHODS 76
3.6.1 "Rotate Beams" method 76
3.6.2 "Rotate Object" Method 79

3.7 REFERENCES 81

CHAPTER 4.0 RESULTS WITH FRINGE COUNTING ANALYSIS 82

4.1. INTRODUCTION 82
4.2 FRINGE COUNTING ANALYSIS OF A CUBE EDGE 83
4.2.1 Rotate Object in clockwise direction 86
4.2.2 Rotate Object in the anti-clockwise direction 94
4.3 FRINGE COUNTING ANALYSIS OF A CYLINDER 97
4.4 REFERENCES 107

5.0 ESPI RESULTS WITH PHASE SHIFT ANALYSIS 108

5.1 INTRODUCTION 108
5.2 PHASE SHIFT ANALYSIS OF A CUBE EDGE 110
5.3 PHASE SHIFT ANALYSIS OF A PYRAMID 113
5.4 CONCLUSIONS 116

CHAPTER 6.0 CONCLUSIONS 117

6.1 PROJECT CONCLUSIONS 117
6.2 RECOMMENDATIONS FOR IMPROVEMENTS AND FURTHER WORK 118

APPENDIX A- EQUIPMENT 120

APPENDIX B- SOFTWARE 123

Chapter 1.0 Introduction

1.1 Optical Metrology

Over the last twenty years or so optical metrology has matured into an important measurement tool for the engineer. Since pioneering work in the early 60's, a variety of interferometric techniques have been developed which are capable of measuring displacements, strain and surface profile. While they have not been the most commonly used nor user friendly methods in the past, with the considerable developments in computing speed, digital image processing and CCD cameras, these techniques are rapidly creating their own niche in the areas of non-destructive testing and surface profilometry.

A metrology system, be it optical or not, must meet the demands of manufacturing, and must also provide accuracy, traceability, speed, reliability, and ease-of-use. As components get smaller and more refined, manufacturing tolerances diminish, putting ever-increasing pressure on the methods being utilised for quality control[1]. Traditional methods which tend to be non-optical have distinct advantages in their own right and are generally designed for a particular application. Optical techniques for surface metrology share the general advantages that the more traditional methods exhibit but also have a great deal more to offer.

An ideal metrology system does not cause damage to the test piece; indeed any contact at all between the object and the measuring equipment is a distinct disadvantage. It is not possible to assume that the contact does not affect the measurements and with some delicate test pieces such as electronic components, the slightest contact can indeed damage the object. Optical techniques are non-contact, giving them a useful advantage over techniques such as ultrasound, acoustic emission, electrical transducers and stylus profilometry. They are also nondestructive, offer high resolution, which in some cases is in the order of nanometres, and are not affected by electromagnetic fields. They also allow full field analysis which is not possible with stylus profilometry and electrical transducers for example.

1.2 Non-destructive Testing (NDT)

1.2.1 Introduction

The purpose of non-destructive testing is to determine whether or not a test component has a flaw or fault, without causing material damage during the test process[2]. In industry today, it is a technology by which different parameters such as material quality and component reliability are monitored. Loading of a particular material and analysis of its behaviour under these loading conditions is one of the main NDT techniques used today. Another test commonly performed is the measurement of crack propagation in a given material. These

tests give engineers in a particular field i.e. structural, mechanical etc. useful information about the durability, reliability and safety of the material of interest. On the production line, non-destructive testing of the product eliminates the need for costly test pieces and the expensive practice of donating a percentage of the product output to testing. Various techniques are utilised to measure and detect the behaviour of a material or component in these situations. Some of these techniques include optical techniques and other non-optical techniques such as acoustic emission[3], x-ray scanning[4], ultrasound[5] and electrical strain gauging[6, 7].

1.2.2 Non optical techniques

1.2.2.1 Acoustic Emission

When subjected to a stress, many materials will emit acoustic waves arising from energy released as the material undergoes plastic deformation and fracture. These waves propagate through the material to the surface where they are detected by highly sensitive piezoelectric transducers. This technique has been used extensively in the study of crack propagation[8].

1.2.2.2 X-ray scanning

While this method finds its applications more in the medical and biological fields, due to the high penetrating capability of X-rays, it is useful when examining almost any structure. The usual method is to use photographic film as the detector, and the X-rays pass through the specimen to the film on the other side[4]. As in medical and biological applications, dark and light regions on the film correspond to variations in the intensity of the rays passing through the object. The differences in intensity will be caused by differences in thickness and density within the object. In this way, sub-surface defects can be detected. One major disadvantage in this technique is the obvious danger to the operator and in medical situations, the object i.e. a patient is also at risk from the X-rays.

1.2.2.3 Ultrasound

In one of the most commonly used techniques in NDT, a transducer which is coupled to a test object emits ultrasonic pulses in the frequency range of 1MHz to 20MHz[6]. These pulses travel through the object and are either reflected, refracted or diffracted by defects or discontinuities in the material. A receiver is used to detect the pulses on the other side of the material, or in most cases the returning echo signal. The amplitude of the signal detected by this receiver will change if a defect is encountered within the object. This technique differs from other NDT methods in that it can trace defects deep within the

material and this is its major advantage. The object can also be examined under no load conditions after damage or wear has already occurred. Disadvantages of the technique however include complex image analysis and the need for direct contact between the object and the transducer. This fact greatly diminishes the versatility of the method.

1.2.2.4 Electrical Transducers

Deformation measurements under loading conditions are usually obtained using strain gauges, which are applied directly to the surface of the object[7]. The strain gauge method works on the principle that a variation in length gives rise to a change in resistance of the strain gauge material, which can be measured using suitable circuitry. Displacement transducers are also used in obtaining deformation measurements[8]. Potentiometric displacement transducers (PDT) and linear variable differential transformers (LVDT) are the two major types. PDT's operate on the principle of a linear variable resistor, i.e. a wiper slides along a resistor track. When a voltage is applied to the transducer, the output-voltage at the wiper is proportional to its position on the resistor track. LVDT's contain a metal push rod fitted with a coil which is moved back and forth between the inductive coils varying the coupling between them. The individual a. c. voltage represents the distance travelled by the core.

A disadvantage of these methods however is the fact that it cannot always be assumed that the presence of the gauges or transducers does not affect the measurements.

1.2.3 Optical Techniques

Optical methods for nondestructive testing have many advantages over the techniques in the previous section. As outlined in section 1.1 they offer full-field analysis without the need for physical contact with the surface to be examined in most cases. They also have high sensitivity and are not affected by electro-magnetic interactions. The main techniques in this area are holographic interferometry[9], moiré methods[10] and speckle techniques[11, 12, and 13].

1.2.3.1 Holographic Interferometry

A holographic recording of a scattering surface can be used to detect the displacement of that surface. The principle of holographic interferometry is that it records the complete pattern of waves reflected by an object both in amplitude and phase by combining this

object wave with an off-axis carrier wave[9]. The interference of these two waves is recorded onto a holographic plate. To enable surface displacement measurement, two of these interference patterns are recorded, one before and one after the object has been displaced. These are then combined to give a fringe pattern which is related to the movement that has taken place. It is possible to view real time fringes by removing the plate after the first exposure, developing it and replacing it in the same position. The holographic image is then reconstructed using the reference beam and any movement of the object will produce interference fringes. The process of developing the plates has seriously curbed the use of this technique in the area of NDT. Even without this problem, the method has an added disadvantage in that it is difficult to measure displacements in different planes independently.

1.2.3.2 Moiré Methods

The moiré effect or a moiré pattern arises when two gratings lie in contact with a small angle between the grating lines[10]. The resulting pattern has a lower spatial frequency than the individual gratings and the exact value of the spatial frequency depends on the angle between the gratings. When measuring in-plane deformations a grating is attached to or projected onto, the test surface. The second grating can be obtained by using straight-line interference fringes of known spacing. This pattern is then superimposed on the object grating. When the surface is displaced the attached grating moves also, producing a moiré

fringe pattern which can be analysed using the usual methods. The main disadvantage of this technique is the contact aspect and so it may not be suitable for some applications.

1.2.3.3 Speckle Techniques

The coherent nature of laser light gives rise to the speckle effect, i.e. the grainy appearance of an optically rough surface when illuminated by a coherent source. The speckle arises because of the random interference which occurs due to the variation in height across the object surface. These surface heights must have a variation of at least the order of wavelength of the laser for the effect to occur. The resultant amplitude at any point in space has a value which varies between zero and a maximum value determined by the magnitudes and phases of the individual contributions from different points. As the point of observation in space is varied, the resultant amplitude and hence the intensity will have a different value. This random intensity variation gives rise to the speckle pattern.[11, 12, 13]

In 1970, Leendertz[14] utilised this speckle effect to measure surface displacements. Since his pioneering work, speckle has evolved into an important tool in optical surface metrology. The speckle techniques in use today can be placed into two classes: speckle photography, where the positional changes of the speckles are measured and speckle interferometry, which measures the change in intensity of the speckle pattern that arises due to deformation.

In speckle photography, light scattered from the object surface is recorded on photographic plates, once before and once after displacement. One recorded speckle pattern is displaced relative to the other by an amount which depends on the amount of displacement and the magnification of the imaging system. The speckle displacement can be determined by illuminating the developed plate with an unexpanded laser beam and examining the far-field pattern. When using an expanded beam and an aperture in the Fourier plane to isolate a particular frequency component, Fourier fringes in the image plane are produced. These fringes can be used to calculate the object's displacement. Both optical set-ups can be seen in Fig. 1.1.

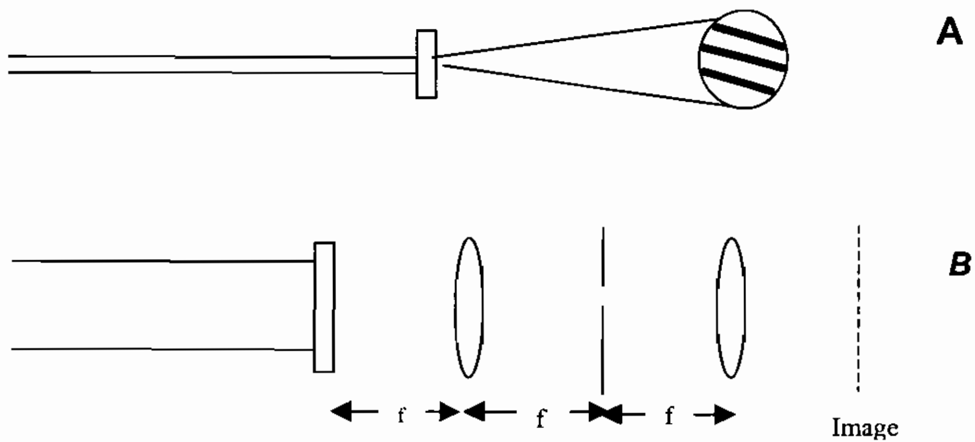

Fig. 1.1. A=Far-field method, B= Fourier Method

The need for development of the photographic plates has limited the use of this technique in the past. However recent advances in digital speckle photography are beginning to change this situation.

In electronic speckle pattern interferometry (ESPI), as in the previous technique, illuminating the object surface to be tested, with laser light forms a speckle pattern. This speckle pattern is imaged onto a CCD array where it is allowed to interfere with a reference pattern. This reference beam may or may not be speckled. The resultant speckle pattern is transferred to a frame grabber on board a computer, where it is saved in the memory and displayed. When the object is displaced, the resultant speckle pattern is different to the first one, due to the change in path difference between the wavefront from the surface and the reference wave. This second speckle pattern is transferred in the same way as the first and is then either added to or subtracted from the original speckle pattern and the result is rectified. The resulting interferogram is displayed as a pattern of bright and dark fringes and it is possible to continuously grab frames and so watch the formation of these fringes in real-time. The fringes are termed correlation fringes since they are obtained through correlation of thc intensities of the resultant speckle interference patterns taken before and after displacement.

The technique was first investigated by Butters and Leendertz[14] at the Loughborough University of Technology as far back as 1971. Since then the method has developed to a highly sophisticated level and has a number of different areas and applications. Depending on the optical configuration of the ESPI system it can be made sensitive to out-of-plane displacements, in-plane displacements, displacement derivatives and surface contour. These systems will be described in detail in Chapter 2.0.

Each type of ESPI system produces a fringe pattern or interferogram, but what these fringes mean depends on the particular system. When measuring displacement, the fringe patterns represent contours of equal displacement and the spacing between the fringes is inversely

proportional to the displacement. Two neighbouring dark or bright fringes represent a displacement whose exact value depends on the wavelength of the light used and the geometrical set-up of the system. The value of this displacement is termed the fringe sensitivity. It is possible to obtain a value for the displacement between two points simply by counting the number of fringes between the points and multiplying by the fringe sensitivity. This was once the only method for analysis before the advent of automatic techniques but it is time-consuming and inaccurate. Today fringe patterns are more likely to be analysed by either the Fourier Transform method or phase shifting, the method used in this project. This latter technique involves producing a fringe pattern which depicts the phase change, (in the range between 0 and 2π) which has occurred between the two speckle patterns. It involves introducing a phase step into the pattern in one of a number of possible ways. This technique and other fringe analysis techniques are discussed in detail in Chapter 2.0.

1.3 Surface Profiling

1.3.1 Introduction

The shape of certain industrial and mechanical components is sometimes of utmost importance when it comes to the performance of the system or environment in which the component functions. Examples of such components are optical components, ball bearings,

certain microelectronic chips and medical devices. From this need for standard or precise shape or profile arises a necessity to provide methods for measuring surface shape, profile and conformity. This class of measurement or metrology is known as profilometry and it can generally be divided into two areas: the measurement of surface roughness and the measurement of surface shape.

1.3.2 Non-Optical methods for profiling

1.3.2.1 Stylus Profilometry

The mechanical stylus is the popular industry standard for the measurement of surface profile[15]. In this method the probe is passed along the surface of the test object, and its movement is converted to a voltage signal by means of a transducer (capacitative, potentiometric etc.). Due to the high precision of the method, it can also accommodate surface roughness measurements. However, the technique has its disadvantages. There is a limited lateral resolution which is obviously dependent on the size of the probe tip, and this results in a loss of surface height information. Also the technique measures along one line of the object and this must be repeated a considerable number of times if the whole object is to be profiled. Whilst this may be reasonable in some cases, with larger objects the process is very time-consuming and perhaps impractical. The major disadvantage of this technique is the fact that the probe must be in direct contact with the object surface. As

described in the previous section, this can sometimes make the method unsuitable for some applications in which the contact can cause damage to the object.

1.3.3 Optical Techniques

1.3.3.1 Introduction

As in the area of NDT, optical methods applied to surface profiling can offer a range of advantages over the traditional methods such as stylus profilometry. They can offer better lateral resolution, whole field analysis and non-contact to combat the problems described in section 1.3.2.1. In addition they can provide high speed analysis and they are non-destructive. Optical profiling techniques can be categorized according to the coherence of the light used. The low-coherence techniques[16] include white light interferometry, coherence radar, coherence scanning and other methods. The principle of all of these techniques is essentially the same, and they differ only in optical set-up and data analysis. A brief description of one of these techniques is included in this section. The other category involves the use of highly coherent sources and techniques in this category include laser profilometry[16], phase shifting interferometry and holographic techniques[2]. The technique relevant to this thesis is the speckle technique for profiling.

1.3.3.2 Low-coherence profiling techniques

As mentioned in the introduction to this section, these techniques have essentially the same principle and so this section will be limited to a brief description of just one, namely coherence radar. This technique detects the occurrence of interference while scanning the object in depth[16]. In a Michelson interferometer set-up, the object takes the place of one of the mirrors. At the beginning of the procedure, the other mirror is positioned further from the beamsplitter than the object. By moving the mirror step-wise closer to the beamsplitter, the reference plane scans the object surface. A pixel output is modulated only when the optical path difference between the reference mirror and the corresponding point on the object surface is less than the coherence length of the light source used. By mapping the point in the scan at which interference occurs for each pixel, a three dimensional image of the surface profile can be obtained.

1.3.3.3 Speckle Profiling Techniques

As described in the section on non-destructive testing, the speckle effect has been utilised in the measurement of displacement and strain. It is also used in the measurement of surface roughness. However, it is also possible to use the speckle phenomenon to measure the profile of an object surface, by ESPI contouring[2]. Contouring is the measurement of

variation in surface height, and hence is the equivalent of profiling. It is possible to achieve this with a number of optical configurations.

Using an out-of-plane system (see Chapter 2), the surface is illuminated sequentially by a master wavefront at two wavelengths λ_1 and λ_2. The difference between the wavelengths is usually of the order of 10nm[2]. In the same way as in the ESPI techniques described in the previous section, the first image is recorded but instead of displacing the object and grabbing the second frame, the wavelength is changed to λ_2 and the second frame is grabbed. This frame is subtracted from the first and a fringe pattern is produced from the result by rectifying it. This pattern represents the variation in phase along the viewing direction between the surface and a plane wavefront and hence represents the surface profile of the object.

For an in-plane ESPI system, the object is illuminated by two beams at equal angles θ, to the normal at the object surface. The phase change in this situation is introduced by either rotation of the object or of the illuminating beams instead of varying the wavelength. At this point the fringe patterns produced by both contouring systems mentioned are analysed in exactly the same way as the fringe patterns from other ESPI systems. A full discussion of these and other variations of ESPI contouring methods is given in Chapter 2.

1.4 Research Objective

The purpose of this research is the design, construction and testing of an ESPI contouring system. It was also an objective of the project that the system be miniature, compact and robust, computer controlled, portable and generally suitable for industrial use. Many of the characteristics just mentioned are required in an effort to overcome the reluctance in industry to adopt these techniques. The portability requirement is an important one since it has been a major disadvantage of these systems when in the past, it has been necessary to bring the test object to the system in the laboratory. This has made these systems entirely unsuitable for certain testing procedures. With the advent of miniature CCD cameras and laser diodes, it has become possible to miniaturize these systems in a way that was previously impossible. Another objective was to utilise user friendly software to control the system to further counteract the inaccessibility mentioned previously.

The project was planned as follows: Initially, an extensive literature review would be conducted in the extensive area of electronic speckle interferometry. Following this, the area of ESPI contouring and profilometry would be concentrated on in particular. Based on this study and the subsequent step of building bench sized versions of systems described in the literature, the contouring system for this project would be designed to comply with the requirements outlined. Sourcing of the necessary equipment would take place at this stage, and finally the miniature system would be assembled. After extensive testing, the system

would be used to obtain results from a particular application, which would then be analysed.

Some building of the bench sized contouring systems took place in the European Commission Joint Research Centre, Ispra, Italy.

1.5 References

1. Selected Papers on Optical Shop Metrology, SPIE Milestone Series, Vol. MS 18, 1992.
2. Jones, R., Wykes C., "Holographic and Speckle Interferometry", Cambridge University Press, 2nd Edition, 1993.
3. Fowler, T.J. "Acoustic Emission testing of glass fibre reinforced composites", International Corrosion Forum, Nace, Houston, Paper 251, March 1992.
4. Aman, J.K. et al "Fundamentals of Radiography, Back to Basics", Materials Evaluation, 36 (4), 24-32, 1978.
5. Williams, J.H. "Ultrasonic evaluation of impact damaged graphite fibre composite", Materials Evaluation 38, 68-72, 1980.
6. Kobayashi, A.S. (Ed.) "Handbook on Experimental Mechanics", Prentice-Hall Publishing, New Jersey, 1987.
7. Megatron Bauelemente "Transducers and Sensors for Linear Motion Measurement", technical data online: http://www.megatron.de/meba/weg/e_weg.htm, August 2000.
8. Prosser, W.H. et al "Advanced wave-form based acoustic emission detection of matrix cracking in composites", Materials Evaluation, 53 (9) 1052-1058, Sept. 1995.
9. Vest, C. M "Holographic Interferometry", John Wiley & Sons, 1979.
10. Gasvik, K. J., "Optical Metrology", 2nd Edition John Wiley & Sons, 1995.

11. Erf, R.K (Ed.) "Speckle Metrology" Academic Press Inc., 1978.

12. Sirohi, R.S. (Ed.) "Speckle Metrology" Optical Engineering Series. Marcel Dekker Inc. Publishing, 1993.

13. Dainty, J.C. (Ed.) "Laser Speckle and related phenomena" Topics in Applied Physics Vol. 9, Springer Verlag, Berlin, 1975.

14. Butters, J.N., Leendertz, J. A., "A double exposure technique for speckle pattern interferometry", Journal of Physics E: Scientific Instruments, 4, 277-279, 1971.

15. Song, J.F., Vorburger, T.V., "Stylus Profiling at high resolution and low force", Applied Optics 30, 42, 1991.

16. Bowe, B "Development and Optimisation of Optical Interferometric techniques for surface metrology", Ph.D. thesis, University of Dublin, June 1999.

17. Shang, J. H., Cai, L.L., "Profilometry using an optical stylus with interferometric readout", Measurement Science & Technology, 8 (5), 546-549, May 1997.

Chapter 2.0 Speckle Techniques and Analysis

2.1 The Speckle Effect

One of the fundamental properties of laser radiation is its coherence[1]. In fact, the high spectral brightness, the monochromaticity and the directionality of a laser beam are properties connected with the coherence of its emission. For two light sources to be mutually coherent they must emit waves of the same frequency that have a constant phase difference which may or may not be equal to zero. Due to this coherent property of light, the phenomenon of interference can occur. Optical interference may be termed as an interaction of two or more light waves yielding a resultant irradiance, whose exact value depends on the phase difference between the component waves.

A diffusely scattering surface, which is illuminated by a coherent source, will produce a grainy light pattern in space[2]. This grainy structure is known as a speckle pattern and it arises because of the random interference of light scattered from the various points on the object surface. The surface must be optically rough, i.e. its surface height variations must be of the order of, or greater than the wavelength of the light source.

As can be seen in Fig. 2.1[3], light is scattered in all directions. These scattered waves interfere to form a pattern consisting of bright and dark speckles, which are randomly

distributed in space. The light forming each individual speckle is fully coherent and can therefore take part in optical interference.

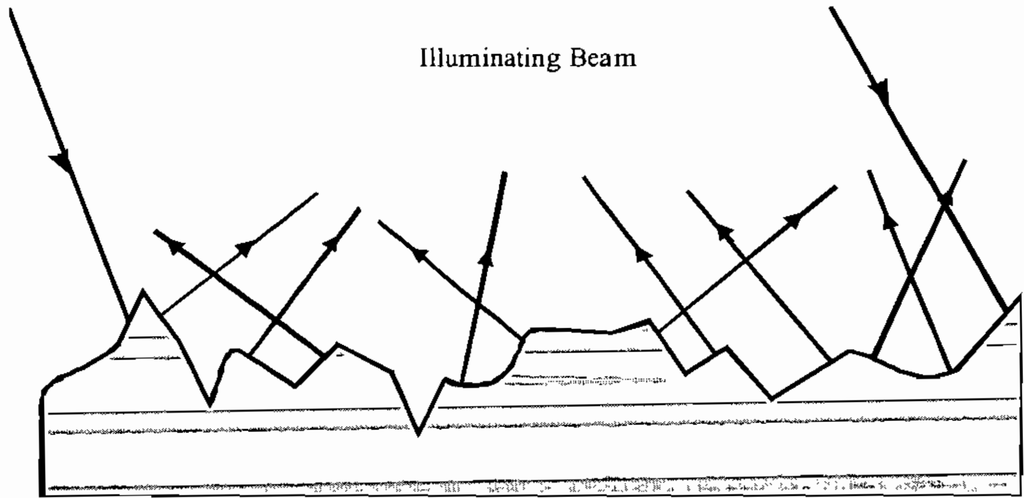

Fig. 2.1: Light scattering from an optically rough surface

The amplitude of the light at any point in space is the sum of the amplitudes of the light contributed from each point on the surface. When a coherent light illuminates an optically rough surface, every point on the surface acts as a source of spherical waves, reflecting the light back. The complex amplitude of the scattered light at any point is the sum of the amplitudes of the contributions from each point. If the resultant amplitude is zero, a dark speckle will be seen, whereas if all the rays arriving at one point are in phase, then an intensity maximum will be seen i.e. a bright speckle.

Fig. 2.2 shows a surface in the x-y plane, whose height at any point (x, y) is given by ξ (x, y). The surface is illuminated by coherent light.

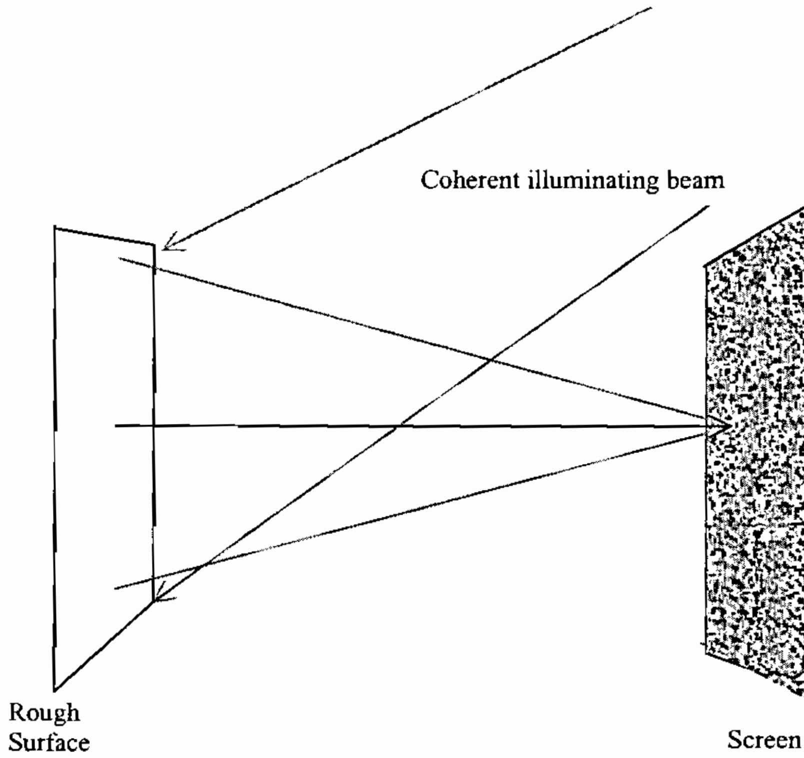

Fig. 2.2 The formation of objective speckle in the S plane

The size of the speckles at any given wavelength, which are observed in the scattered light, depends on the distance from the surface and the size of the illumination area. Therefore the spatial frequency of the speckle increases as the illuminated area increases. The complex amplitude U, at a point (x', y') in space, at a distance *i* from the surface may be written as[4]

$$U(x',y') = k\int_{-\infty}^{\infty}\int a(x,y)\exp\left[\frac{2\pi i}{\lambda}G\xi(x,y)\right]dxdy \qquad 2.1$$

Where k is a constant, a (x, y) is the complex amplitude of the light incident at (x, y) and G is a geometrical factor associated with the illumination and viewing directions. The integration is over the whole illuminated surface. Because the surface height varies randomly, the resultant amplitude also varies with (x', y'). The resultant amplitude has a value which varies between zero and a maximum value determined by the magnitude and phase of the contributing amplitudes. As the point in space is varied, the resultant amplitude will have a different random value and thus the intensity will vary randomly. This varying intensity effect is known as the speckle effect.

Goodman[5] gives a detailed account of speckle statistics, and so only the results will be given here. It can be shown that the standard deviation, σ of the intensity is given by

$$\sigma = \langle I \rangle \qquad 2.2$$

where $\langle I \rangle$ is the mean intensity. The intensities at two points on the speckle pattern will be closely related when the points are close to one another. As they move apart, the intensities become unrelated. R, the autocorrelation function, provides the relationship between the intensities at the two points as a function of the distance between them. When the distance between them equals zero, $R = \langle I^2 \rangle$. The distance at which the intensities become unrelated provides an estimate for the size of the speckles. Goodman derived an expression for the autocorrelation function, where the surface, of dimensions L x L, is illuminated by a uniform beam. From this, the average size of a speckle is found to be

$$(\Delta x) = \frac{\lambda z}{L} \qquad 2.3$$

where z is the distance between the viewing and object planes. Thus, the speckle size is inversely proportional to the size of the illuminated area. This type of speckle is known as objective speckle since its size depends only on the plane in space where it is viewed.

When an image is formed of the illuminated surface, the image is a similar pattern. In this case however, the size of the speckles in the image plane is dependent on the aperture of the viewing system and the distance from the lens to the image plane. In Fig. 2.3 below, a point P_1 on the surface is imaged onto the image plane S, forming a diffraction pattern centred at S_1.

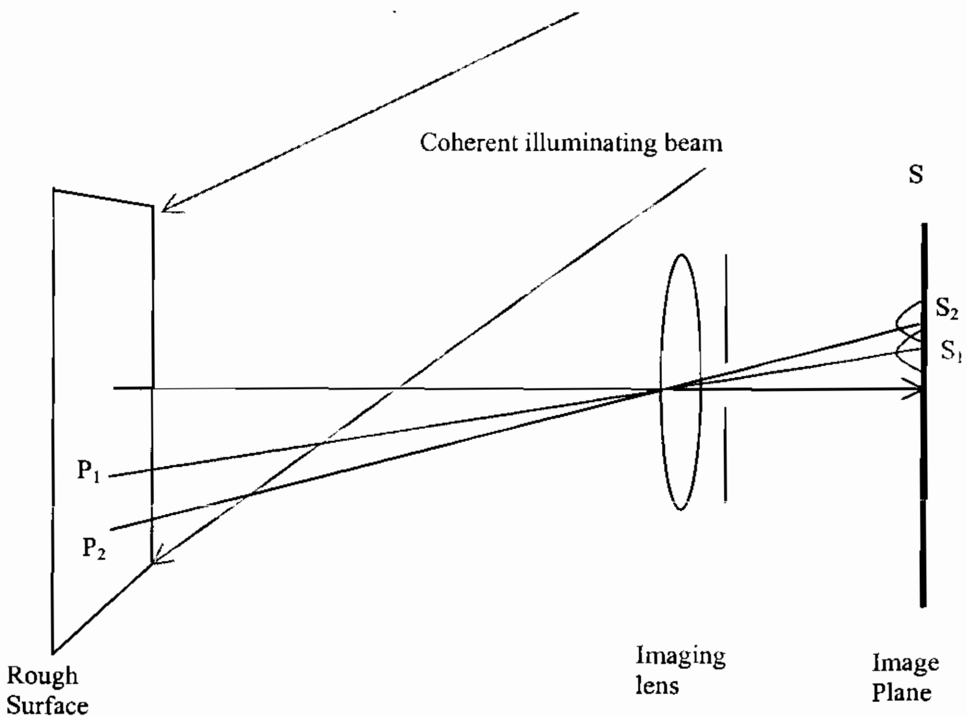

Fig. 2.3 The formation of subjective speckle in the S plane

Points around P_1 will produce similar diffraction patterns which will in turn overlap onto S_1. The amplitude will be different for each diffraction pattern as the light from each point on the surface has a random phase produced by the random variations in surface height. The point P_2 makes no contribution to the complex amplitude at S_1 as the diffraction pattern it produces has its first minimum overlapping with S_1. The contributions from points further away from P_1 than P_2 are negligible, as the secondary maxima of the patterns are much smaller than the primary maxima. Therefore, the intensity of the light at the point S_1 is the sum of the intensity contributions from an area centred around P_1 with a diameter d given by twice the distance from P_1 to P_2. The distance d on the image plane between S_1 and S_2 can be derived from diffraction theory as

$$d = \frac{1.22\lambda v}{a} \qquad 2.4$$

Where a is the diameter of the viewing lens aperture and v is the distance from the lens to the image plane. Thus the size of the speckle in the image plane is given by

$$d_{sp} = \frac{2.4\lambda v}{a} \qquad 2.5$$

This corresponds to an object size of

$$d_{obj} = \frac{2.4\lambda u}{a} \qquad 2.6$$

And u is the distance from the lens to the object.

Thus the size of the speckles in the image plane depends on the aperture of the imaging lens. Hence it is termed subjective speckle. The light rays contributing to any one speckle can only come from a limited area on the object i.e. the object speckle size. Objective speckle differs in that light from the entire illuminated surface contributes to every speckle.

The speckle effect was initially regarded as a nuisance to those working with lasers in the early days. However in 1970, Leendertz[6] demonstrated the use of speckle to measure surface displacements and since then, it has become an important tool in the area of optical surface metrology. Today, there are many different techniques based on the speckle effect and these can largely be categorised under two headings: 1) Speckle Photography which measures the positional changes of the speckles and 2) Speckle Pattern Interferometry which measures intensity changes caused by phase changes. These topics will be covered in depth in the following sections.

2.2 Speckle Photography

In speckle pattern photography, a viewing lens collects light scattered from an optically rough surface in its undisplaced and displaced positions[4]. A recording is made of the two scattered fields on a single photographic plate. The two scattered fields can be assumed to be identical, except that one will be displaced with respect to the other by an amount that depends on the object displacement. If the relative displacement of the two speckle

patterns can be determined, the displacement of the object can be determined. This can be determined from the Fourier Transform of the doubly exposed photograph as described in Chapter 1.

As stated previously, speckle photography measures the positional changes of the speckles. It is by far the simplest speckle technique in terms of set-up, incorporating merely a camera, a laser and the object. Fig. 2.4 shows a speckle photography set-up.

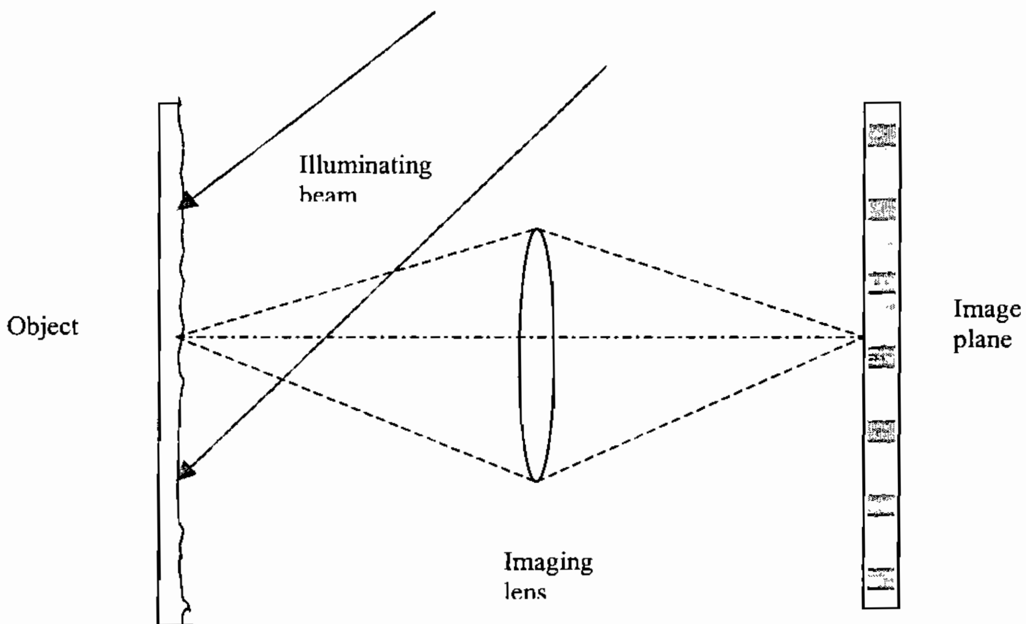

Fig. 2.4 Speckle Photography Set-up.

The general procedure is to expose a photographic plate to two displaced speckle patterns, one before and one after the object has been moved. Alternatively it is also possible to record the two speckle patterns on different plates and subsequently to superimpose one on the other to eliminate the effect of rigid body movements undergone during deformation.

The recorded specklegram is analysed in one of the following ways: the first method is a point by point approach using a narrow laser beam. Diffraction of this beam by the speckles lying in the beam area gives rise to a diffraction halo, which is modulated by an equispaced system of Young's fringes. Displacement is inversely proportional to fringe spacing. The second method involves obtaining the Fourier Transform of the doubly exposed photograph. Using this technique, the photograph is imaged through a lens and a spatial filter is used to allow a particular spatial frequency through. The fringes are formed in the Fourier plane of a second lens[7].

2.3 Speckle Pattern Correlation Interferometry

2.3.1 Basic Principles of Interferometry

Consider the interferometer in Fig. 2.5. A plane wavefront U_o is split into two components of equal intensity by the beamsplitter B[4].

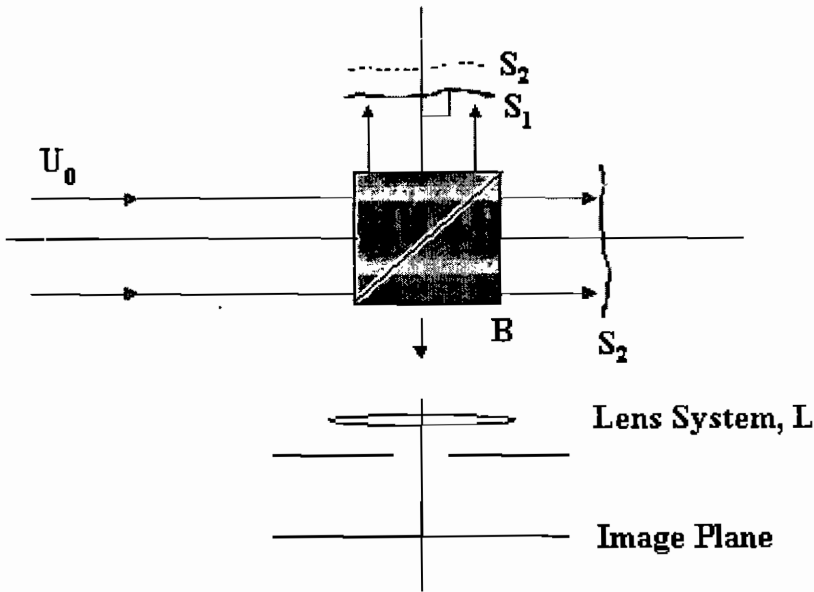

Fig. 2.5: The Michelson arrangement of out-of-plane displacement sensitive speckle pattern correlation interferometer

Thesc two beams illuminate the surfaces S_1 and S_2. The wavefronts scattered from S_1 and S_2 interfere on recombination at the beamsplitter and the result is recorded at the image plane of the lens aperture combination, L. The intensity distribution in this image plane is given by[8]:

$$J_1 = I_1 + I_2 + 2\sqrt{I_1 I_2} Cos\,\psi \quad 2.7$$

Where I_1= Intensity from wavefront 1, I_2= Intensity from wavefront 2, Ψ = A phase term.

It is important to note that in the above expression Ψ is random, i.e. it depends on the surface height variations, and therefore the resultant intensity varies for each point across the surface.

When S_1 is displaced a distance d normal to the surface, i.e. out-of-plane, a phase change $\Delta\phi$ arises[1]:

$$\Delta\phi_d = \frac{4\pi d}{\lambda} \tag{2.8}$$

Where λ is the wavelength of the light source used.

This changes the intensity at the point to:

$$J_2 = I_1 + I_2 + 2\sqrt{I_1 I_2}Cos(\psi + \Delta\phi_d) \tag{2.9}$$

By correlating the intensities J_1, and J_2. (See Ref. 1, Appendix E) it can be shown that when

$$\Delta\phi = 2n\pi \tag{2.10}$$

J_1 and J_2 have maximum correlation. The correlation coefficient is zero, i.e. J_1 and J_2 become uncorrelated when

$$\Delta\phi = 2(n+1)\pi \tag{2.11}$$

So, maximum correlation exists where $d = \frac{1}{2} n\lambda$ and minimum correlation exists where $d = \frac{1}{2}(n + \frac{1}{2})\lambda$.

Therefore, the variation in correlation represents the variation in the displacement of the object surface, d. Maximum correlation occurs when no displacement occurs and a bright fringe can be seen. A dark fringe is seen when minimum correlation occurs.

2.3.2 Electronic Speckle Pattern Interferometry (ESPI)

The resolution of the recording medium used in speckle techniques need only be low compared with that required in holography since it is only necessary to resolve the speckles, and not the very fine fringes formed by the interference of object and reference beams in holography[8]. Therefore a standard television or CCD camera may be used to record the pattern. In this case, the method is known as Electronic Speckle Pattern Interferometry (ESPI) and was first demonstrated by Butters and Leendertz[15]. The main advantage of this method over the one described previously is that it enables real-time correlation fringes to be displayed directly on a monitor without the tedious photographic processing.

ESPI is based on the coherent addition of a subjective speckle pattern which is scattered from an object and a reference field. The intensity of the resultant speckle pattern is dependent on the relative phase distribution of the added fields. Deformation or surface displacement causes a change in the intensity of the resultant pattern. Addition or subtraction of the new pattern from the first one produces a fringe pattern representing the surface displacement. Subtraction is the most commonly used method since it largely eliminates background noise. In this subtraction process, the CCD signal corresponding to the interferometer image-plane speckle pattern of the undisplaced object is stored electronically. The object is then displaced and the live image, detected by the CCD camera, is subtracted from the stored image. The output is then rectified and displayed on a monitor where the correlation fringes may be observed live. This technique is the basis of many different types of ESPI systems, which differ in their optical configuration and sensitivity, but which all produce a fringe pattern in the manner just described. The following section examines the different types of ESPI systems, particularly the one relevant to this thesis, the ESPI contouring system.

2.4 ESPI Systems

In the interferometer described in 2.3.1, fringes are produced which represent contours of constant out-of-plane displacement[8]. The phase difference $\Delta\phi$ which gives rise to the variation in correlation between the two speckle patterns may be made sensitive to different components of surface displacement. This is achieved by altering the object and reference

beam geometries. This section deals with the various speckle interferometers for which $\Delta\phi$ is a function of in-plane displacement, out-of-plane displacement and out-of–plane displacement gradients. Arrangements are also described which are sensitive to shape, for three- dimensional profilometry.

2.4.1 In-Plane ESPI

Speckle interferometers for measuring the in-plane component of displacement all work on the principle that the surface under investigation acts as both of the scattering elements in the equivalent Michelson-type interferometer. Leendertz first demonstrated this, by illuminating the surface with two beams of coherent light incident at equal angles θ on either side of the normal as in Fig. 2.6. The light scattered is focused by a lens onto a photographic plate or a CCD array. Each illuminating beam generates its own speckle pattern and the two combine on the plate or array. If the surface now moves in the z direction, i.e. normal to the plane, the two interfering beams will undergo equal path length changes and the combined speckle pattern in the image formed by the lens will remain unchanged.

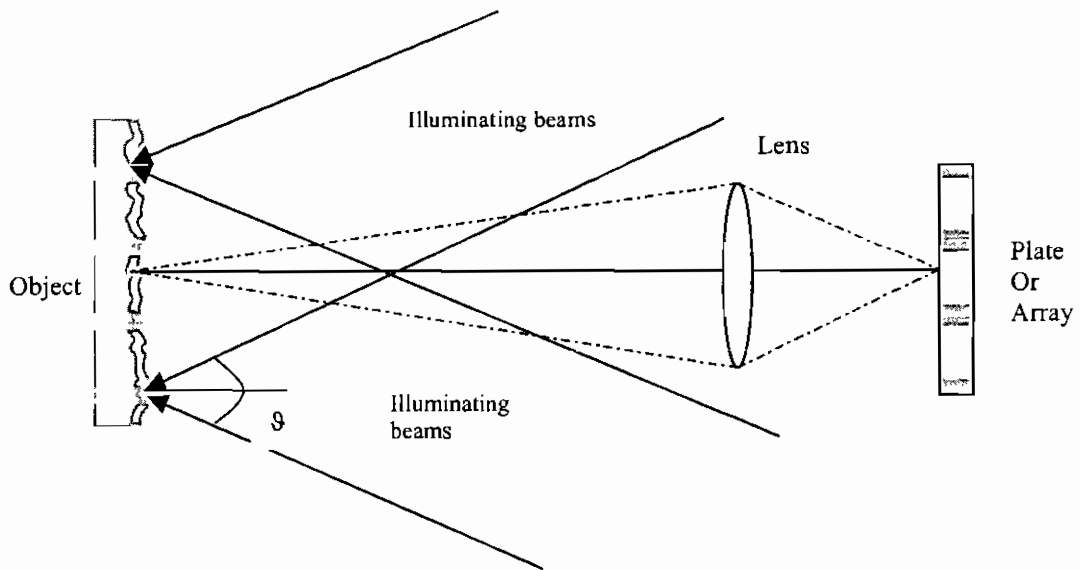

Fig. 2.6 In-Plane ESPI system

However, if the surface becomes displaced by a small distance d in the x-direction (defined by the intersection of the surface plane and the illuminating beams) one path length will be increased by dsinϑ, while the other will be decreased by the same amount. Correlation of the combined speckle pattern with the original pattern before displacement will occur when

$$2d\sin\vartheta = n\lambda \qquad 2.12$$

where ϑ = angle of incident of the illuminating beam

Subtraction and rectification will generate a fringe pattern related to the component of surface displacement in the x direction. The spacing of the fringes corresponds to an incremental displacement of $\lambda/(2\sin\vartheta)$, so that the sensitivity of the interferometer can be varied by altering the incident angle of the illuminating beams. For example, in an

interferometer with an illuminating angle of incidence of 45°, the sensitivity will be 0.7 times the wavelength per fringe. By plotting the fringe positions as a function of x, the linear strain $\delta d_x/\delta x$ may be derived.

2.4.2 Out of Plane ESPI.

In an out-of-plane ESPI system the object is viewed normal to the surface and illuminated by one beam, the object beam, at an angle near to normal. The resulting speckle pattern is imaged onto the CCD array where it interferes with a reference beam[8]. The reference beam is aligned with the light coming from each particular part of the surface being examined. The ESPI subtraction fringe patterns that are produced represent contours of equal displacement along the viewing direction.

The optical configuration of the original Leendertz ESPI system is shown in Fig. 2.7. It is similar to the Michelson interferometer but the mirrors have been replaced with specular surfaces. Leendertz used a photographic plate in the image plane and used a double exposure technique to obtain fringes by addition. The resultant speckle pattern in the image plane is formed by the interference of the two speckle fields scattered from the surfaces. The surfaces are illuminated by collimated light, normal to the surface. The distance from the image plane to the object along the optical axis is d_0. When one of the surfaces is

deformed, the relative phase change between the waves at a point (x, z) in the image is given by[8]

$$\Delta\phi = \frac{4\pi d}{\lambda}\left(1 - \frac{x^2 + y^2}{4d_0^2}\right) = n\lambda \qquad 2.13$$

where it is assumed there is virtually no movement of the surface in the x and y planes, and d is the displacement along the z-direction. From this equation, it is clear that the fringes obtained are only contours of equal out-of-plane displacement for the points lying close to the optical axis. A correction term for each point (x, z) is needed

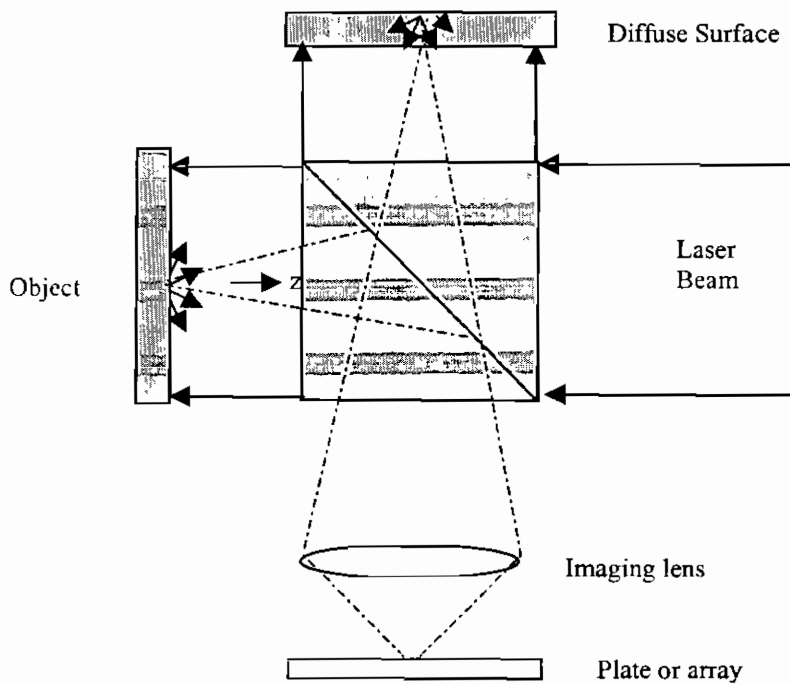

Fig. 2.7 The schematic of the Leendertz out-of-plane ESPI system.

when analysing the fringes. Thus, the phase change between the two fields at any point on the image can be given by[3]:

$$\Delta\phi = \frac{4\pi d}{\lambda} = n\lambda \qquad 2.14$$

where n is the fringe order number. Maximum intensity correlation, between the images taken before and after deformation, occurs when $\Delta\phi = 2n\pi$ and minimum correlation occurs when $\Delta\phi = (2n + 1)\pi$. When the system is used with a CCD camera, the frame taken before deformation is subtracted from the frame after, and the result rectified, producing a fringe pattern.

Areas of maximum correlation are seen as dark fringes and correspond to a displacement of

$$d = \frac{n\lambda}{2} \qquad 2.15$$

Areas of minimum correlation are seen as bright fringes and occur in areas where the out-of-plane displacement is

$$d = \frac{(n + 1/2)\lambda}{2} \qquad 2.16$$

Two neighbouring dark fringes represent points whose relative phase shift is 2π, so from the above equation they represent a relative out-of-plane displacement given by

$$d = \frac{\lambda}{1 + \cos\theta} \qquad 2.17$$

2.4.3 Shearing ESPI (Shearography)

The potential of speckle techniques for the measurement of the derivatives of surface displacements[8] was proposed by Butters and Leendertz[15] and by Hung and Taylor[9]. The principle behind this class of methods is the same as that of speckle interferometry, except that the two interfering speckles now originate from the same object and are sheared laterally with respect to each other. Fig. 2.8 is a schematic of the Butters and Leendertz Michelson type of shearing interferometer. The object is illuminated by a beam which is in the xz plane and makes an angle ϑ with the surface normal. It is imaged through a Michelson interferometer. A small tilt of one of the two mirrors introduces a lateral shift δx between the two speckle patterns.

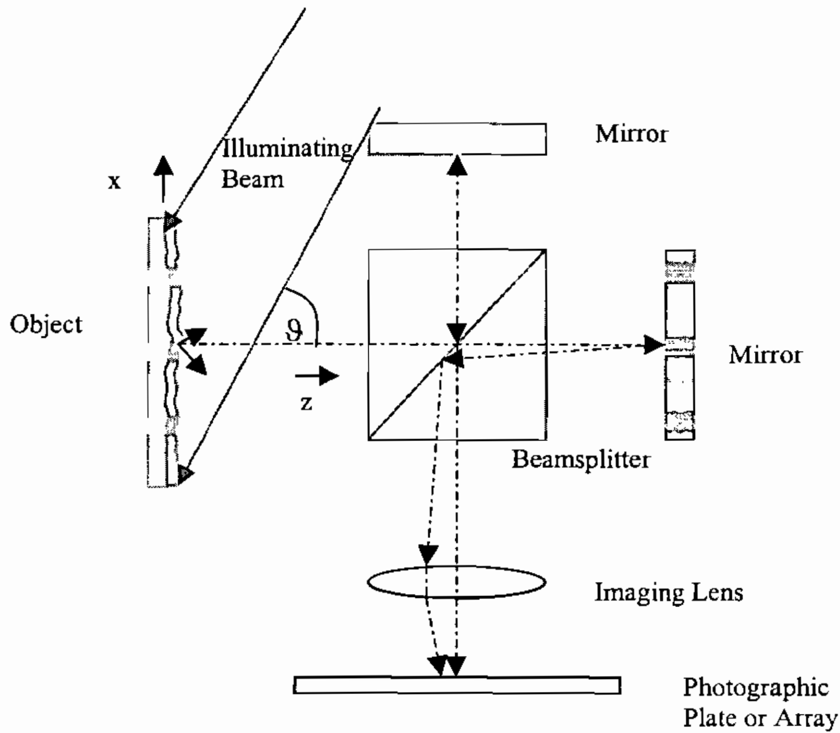

Fig. 2.8 Speckle Shearing system

When the object is deformed, an arbitrary point (x, y) on the object surface is displaced to (x+u, y+v, w) and a neighbouring point (x+δx, y) is displaced to ((x+δx+u+δu, y+v+δv, w+δw). Then the relative path length change due to the displacement between the two contributing points is given by[8]:

$$\Delta\tau = \delta x\left[\left(Sin\vartheta + \frac{x}{d_0} - \frac{x^2+y^2}{2d^2{}_0}\right)\frac{\delta u}{\delta x} + \frac{y}{d_0}\left(1 - \frac{x^2+y^2}{2d^2{}_0}\right)\frac{\delta v}{\delta x} + \left(1 + Cos\vartheta - \frac{x^2+y^2}{2d^2{}_0}\right)\frac{\delta w}{\delta x}\right] \quad 2.18$$

where d_0 = distance from the image plane to the object along the optical axis.

(The terms containing the product $u\delta x$, $v\delta x$ and $w\delta x$ have been neglected in writing Equation 2.18.)

In an optical set-up designed to make the angle subtended by the imaging lens at the object surface small, d_0 is usually large compared with x and y and the equation reduces to[3]:

$$\delta x\left[Sin\,\vartheta\frac{\delta u}{\delta x}+\left[\left((1+Cos\,\vartheta)\frac{\delta w}{\delta x}\right)\right]\right]=n\lambda \qquad 2.19$$

Various arrangements for the implementation of different shear types namely: lateral, radial, rotational, inversion and folding have been reported. In fact, Ganesan et al[10] presented a universal digital speckle shearing interferometer which yield all of the above shear types.

Advantages of the shearing system are obvious when it is considered that speckle techniques measure surface displacements. Strèss analysts are usually interested in strain measurement, which is proportional to the first derivative of the displacement. A speckle shearing system measures directly the derivatives of the displacements, and since no reference wave is used, the technique has considerable tolerance to environmental disturbance. Other advantages of shearing techniques include simplicity of set-up and also a controllable range of sensitivity. Adjustment of one of the mirrors introduces either an increase or decrease in the amount of shear and a subsequent increase or decrease in sensitivity.

2.4.4 ESPI Contouring (Profilometry)

As with other speckle techniques, there are several different optical configurations which will give rise to fringes which represent surface profile[8]. Fig. 2.9 shows the two-beam illumination method for contouring proposed by Ganesan and Sirohi.[11] The specimen is illuminated by two beams incident at equal angles ϑ to the optical axis.

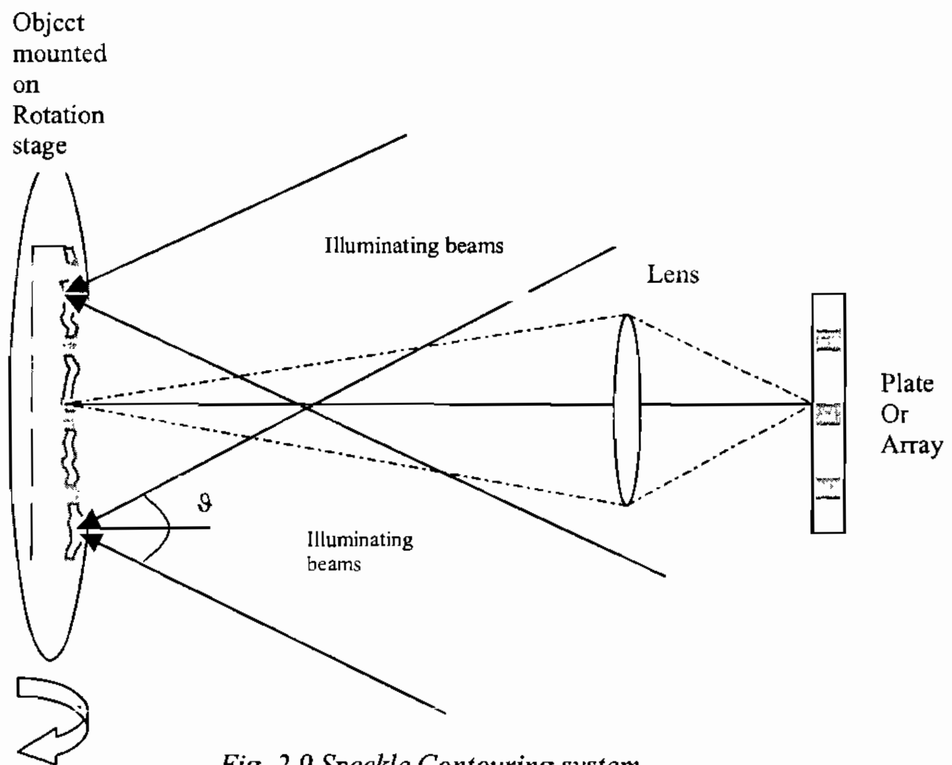

Fig. 2.9 Speckle Contouring system

The speckle pattern in the image plane arises from the superposition of the individual patterns generated by the two beams. In this set-up, either the object or the beams can be

rotated to give rise to contour fringes. However in the arrangement of Ganesan and Sirohi, the object was rotated by an amount $\Delta\vartheta$ around an axis perpendicular to the plane containing the two illumination beams. For this set-up the relative phase change introduced in the interferometer as a result of the particular rotation is given by[8]:

$$\Delta\phi = \frac{4\pi}{\lambda}\sin\vartheta\sin\Delta\vartheta \qquad 2.20$$

Where λ is the wavelength of the laser illumination. The increment of height between two contour planes, i.e. the system sensitivity, is then given by:

$$\Delta z = \frac{\lambda}{2\sin\vartheta\sin\Delta\vartheta} \qquad 2.21$$

Another method for surface contouring is the wavelength modulation method, where the wavelength of the illuminating beam is altered between exposures or frames. In this case, the contour sensitivity per fringe is given by[4]:

$$\Delta z = \frac{\lambda_1\lambda_2}{2(\lambda_1 - \lambda_2)} \qquad 2.22$$

Yet another method involves a Michelson type set-up, where one of the mirrors is replaced by the 3-dimensional object and the other by a scatter surface. The object is placed in an immersion tank filled with a transparent liquid of refractive index n'. A change in the

refractive index of the liquid, between two exposures or frames induces a relative phase change in the interferometer related to the topographic variations of the specimen surface. In this situation, the height difference corresponding to neighbouring fringes is[8]:

$$\Delta z = \frac{\lambda}{2(n''-n')} \qquad 2.23$$

Where n" is the new refractive index of the liquid.

As with all the other ESPl systems: in-plane, out-of plane and shearing, an ESPI contouring system produces a fringe pattern. To analyse the fringe pattern, one of a number of techniques must be utilised. The major techniques and particularly the ones used in this thesis are described in the following section.

2.5 Fringe Analysis

2.5.1 Introduction

A fringe pattern or interferogram, is the primary result obtained from each type of ESPI system. Qualitative analysis of these patterns in the form of visual inspection can sometimes be sufficient, as in the case of defect or crack detection and in the past this was the only method of analysis available. However, with the development and decreasing cost of digital image processing equipment, digital fringe analysis techniques have been developed to an extremely high level in recent years. This has been instrumental in the more widespread use of techniques like ESPI in both the laboratory and industry. There are two automatic techniques to be discussed: the earlier intensity-based techniques and more recently, phase-measurement techniques.

2.5.2. Intensity based techniques

Before the development of the phase-measurement techniques discussed in Section 2.5.3, intensity based techniques were the only image-processing tools available for the automatic analysis of interferograms. They are still important methods in that they are the only viable methods at times such as when fringe patterns are obtained from old photographic records

or when results are obtained from interferometric systems not suited to the application of phase-measurement techniques. In a situation where quantitative results are not needed, they are particularly appropriate.

For this group of techniques it is very important to minimise the level of noise[3], including speckle noise and therefore pre-processing in the form of filtering is advisable. Most commonly, low-pass filtering and median filtering are the techniques used. Another method is to combine two fringe patterns of opposite phase. By subtracting one from the other the noise will be cancelled while the fringes will combine to give a higher contrast than the original. There are two main intensity based techniques which will be covered here: 1) Fringe counting and 2) Automatic fringe location

2.5.2.1 Fringe Counting

This method of fringe analysis is inferior, in terms of accuracy, to the methods to be described later on, but in the absence of other means of analysis, it can be quite useful and effective. The method involves observing the formation of the fringe pattern and noting particular parameters while doing so. The most important of these must be the fringe order

number n. Fig. 2.10 shows a fringe pattern obtained using an ESPI contouring system, with the order numbers assigned.

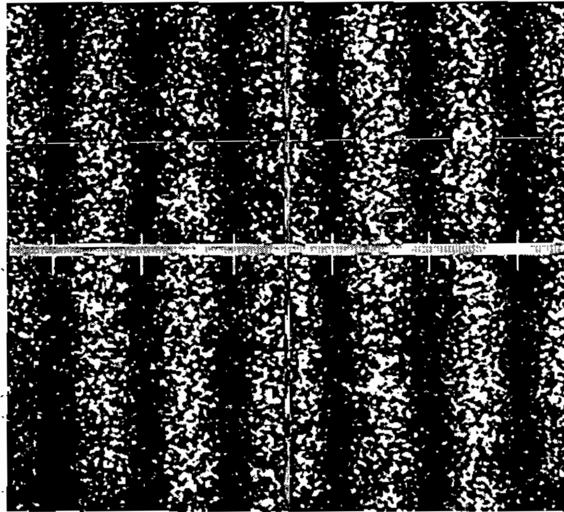

1 2 3 3 2 1

Fig. 2.10 ESPI Contouring Fringe pattern (simple cube edge) with order numbers assigned and fringes midpoints marked off for analysis

By placing a scale over the image and viewing it through the lens system it is possible to determine exactly what area is imaged. In the case of the above fringe pattern, the imaged area was 38 mm square. The pattern that is produced is known to cover 512 x 512 pixels. Using this data it is possible to calculate the positions of the fringes in the following manner.

The fringe pattern is opened in an image processing package called Scion Image (see Appendix A). Within this package it is possible to set a millimetre per pixel scale. It is then possible to read off the x-axis positions of the fringes by marking the exact centre of each and noting the corresponding position in the mm scale.

To obtain the height information from the fringe pattern, the fringe orders are required. The value of fringe sensitivity, Δz, is determined from Equation 2.21. To do this, ϑ the illuminating angle and $d\vartheta$ the rotation which has taken place must be noted. For this example, $\vartheta = 12.5\,°$ and $d\vartheta = 0.0155\,°$, giving a Δz value of 6.7mm, where $\lambda = 785$nm.

The height information is determined by multiplying this value of Δz by the fringe order number. The result is a series of x-position values with a series of corresponding height values. When plotted, these values produce a graph, which represents the surface shape.

The method, while time consuming and inaccurate, has an advantage over more sophisticated methods in that it does not require very high contrast in order to produce quantitative results. However it merely provides information for points located along fringes and so for whole-field and more accurate analysis, an automatic technique such as described in the latter sections of this chapter, is necessary.

2.5.2.2. Automatic fringe location

When interferometric techniques are used for non-destructive testing or inspection, it is sometimes possible to design a relatively simple fringe analysis system[3]. After identifying the characteristics of the fringe pattern which are significant in the application, the capabilities of the analysis system can be confined to those required for the measurement in question. Many specialised fringe analysis procedures can be developed by utilising prior knowledge of the fringe pattern. An example of this is discussed by Gasvik[3] where holographic interferometry is applied to the testing of honeycomb panels. Brazing is a procedure whereby two pieces of metal, in this case the honeycomb panels, are joined together by heating to red heat and using a high melting point solder such as copper, zinc, or brass.

Debrazing of the honeycomb panels produces groups of nearly circular fringes. The procedure starts with counting the number of fringes along a number of horizontal lines through the image as in Fig. 2.11 below.

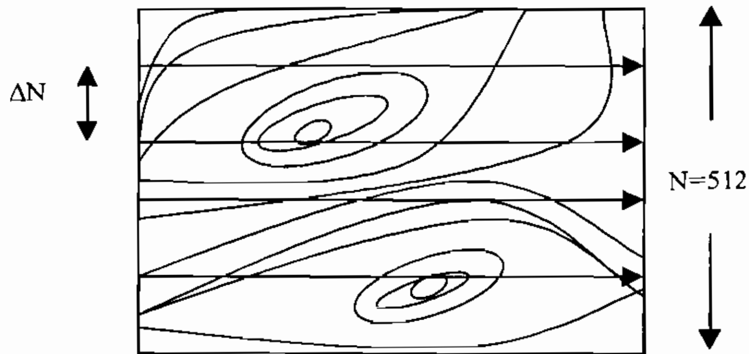

Fig: 2.11 Count fringe peaks along horizontal vectors

When a comparatively large number of fringes appear on a given line, a flaw is presumed to exist on that line. Short vertical scans across the line in question are then used to search for the location of the flaw by looking for a comparatively large number of fringes in the vertical direction as in Fig. 2.12.

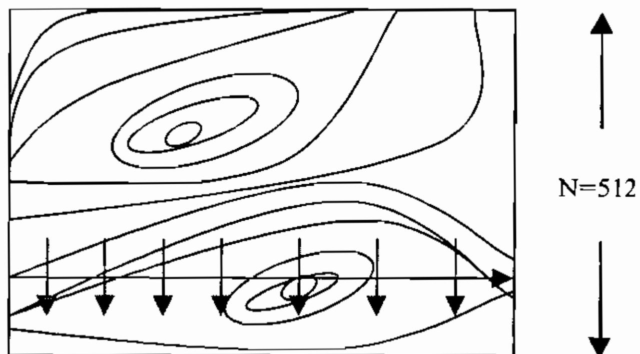

Fig. 2.12 Count peaks along vertical vectors

Having identified the probable existence and location of a flaw, the system carries out a further check by counting fringes along each of four short vectors angularly spaced at 45

degrees, centred on the probable flaw site. (Fig. 2.13) If the same number of fringes appear on each of the four vectors, then the existence of a flaw is confirmed.

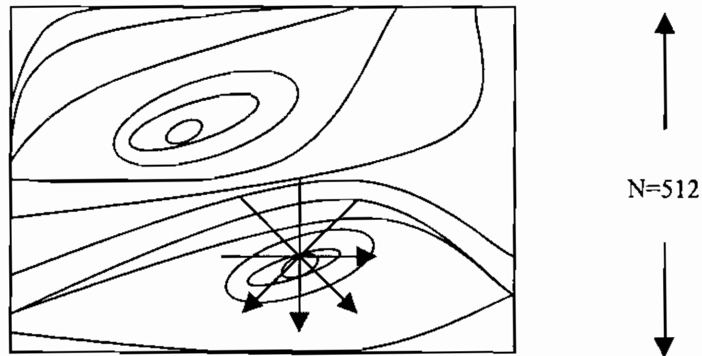

Fig.2.13 Scan at 0°, 90°, 45°, 135°

There are several other intensity based methods of fringe analysis which are discussed by Gasvik. However, the techniques in the following section have become the more commomly used methods due to their greater accuracy and speed.

2.5.3 Phase-Shifting

The direct measurement of phase information has many advantages over simply recording interferograms and digitising the position of fringe maxima and minima, the basis of the

techniques in the previous section. The precision of phase measurement techniques is far greater and the process is relatively simple[13, 14].

Phase shifting is based on the introduction of a temporal phase shift, between the object and reference beams in the interferometer and this results in a movement of intensity peaks across the pattern. This phase shift is introduced in calibrated phase steps or as continuous periodic phase modulation. The phase change itself may be implemented in a number of ways: a displacement of a mirror, a tilt of a glass plate, elongation of an optical fibre, electro-optical modulation, or a refractive index change. The method particular to this thesis is described in Chapter 3. Many different phase shifting algorithms have been developed, each producing another fringe pattern with considerably less noise than the original. The fringes loose their sinusoidal characteristic and begin to resemble ramp waves.

All of the phase shifting algorithms eliminate background terms by simple arithmetic or trigonometric operations on the acquired images. It is imperative however, that the speckles are perfectly still and so these techniques are only effective in the absence of mechanical or thermal instability. The most common phase shifting technique is one in which the phase in one arm of the interferometer is stepped in N equal and controlled steps so that the total phase shift is 2π.

By combining the resulting N+1 images it is possible to solve for ϕ, the phase at each pixel. If N=3, four frames are grabbed $\pi/2$ apart and ϕ can be calculated for every pixel. Phase shifts $\pi/2$, π, $3\pi/2$ produce the following four equations:

$$\begin{aligned}
I_1 &= I_1 + I_2 + 2\sqrt{I_1 I_2}\cos\phi \\
I_2 &= I_1 + I_2 + 2\sqrt{I_1 I_2}\cos(\phi + \pi/2) \\
I_3 &= I_1 + I_2 + 2\sqrt{I_1 I_2}\cos(\phi + \pi) \\
I_4 &= I_1 + I_2 + 2\sqrt{I_1 I_2}\cos(\phi + 3\pi/2)
\end{aligned} \qquad 2.24$$

Using the following algorithm[13]:

$$\frac{I_4 - I_2}{I_1 - I_3} \qquad 2.25$$

gives rise to:

$$\frac{I_4 - I_2}{I_1 - I_3} = \frac{\sin(\phi)}{\cos(\phi)} = \tan\phi \qquad 2.26$$

Which leads to:

$$\phi_{(x,y)} = \tan^{-1}\left[\frac{I_{4(x,y)} - I_{2(x,y)}}{I_{1(x,y)} - I_{3(x,y)}}\right] \qquad 2.27$$

This process produces an image in which the intensity value at each pixel represents the phase at that pixel in the reference image. However, since the inverse tan function gives values between $-\pi/2$ and $+\pi/2$, the phase cannot be directly evaluated over a 2π interval.

The object is then displaced and a new image is grabbed. Again the phase of one beam is stepped N times and at each step, an image is grabbed. By combining the resulting N+1 images and using the same algorithm, it is possible to solve for $\phi+\Delta\phi$, where $\Delta\phi$ is the phase change at each pixel caused by the surface displacement. This results in another intensity value at each pixel which represents the phase at that pixel in the image which was taken after displacement. The two phase images are then subtracted from one another to produce a resultant image containing the phase information $\Delta\phi$. This image is a fringe pattern where the intensity value at each pixel represents the phase change at that pixel caused by the surface displacement.

2.5.4 Phase Unwrapping

The previous section has discussed a typical method for determining the phase term in a fringe pattern. This and all other methods result in an equation of the form:

$$\phi = \tan^{-1} (C/D) \qquad 2.28$$

(where C / D represents the frame intensity algorithm)

Because of the multi-valued $\tan^{-1}$ function, the solution for ϕ is a saw-tooth function (see Fig. 2.14(a)) and discontinuities occur everytime ϕ changes by 2π. The term phase unwrapping arises because the final step in the fringe pattern measurement process is to unwrap or integrate the phase along a line (or path) counting the 2π discontinuities and adding 2π each time the phase angle jumps from 2π to 0 or subtracting 2π if the change is from 0 to 2π. Fig. 2.14 (b) shows the data in Fig. 2.14 (a) after unwrapping.

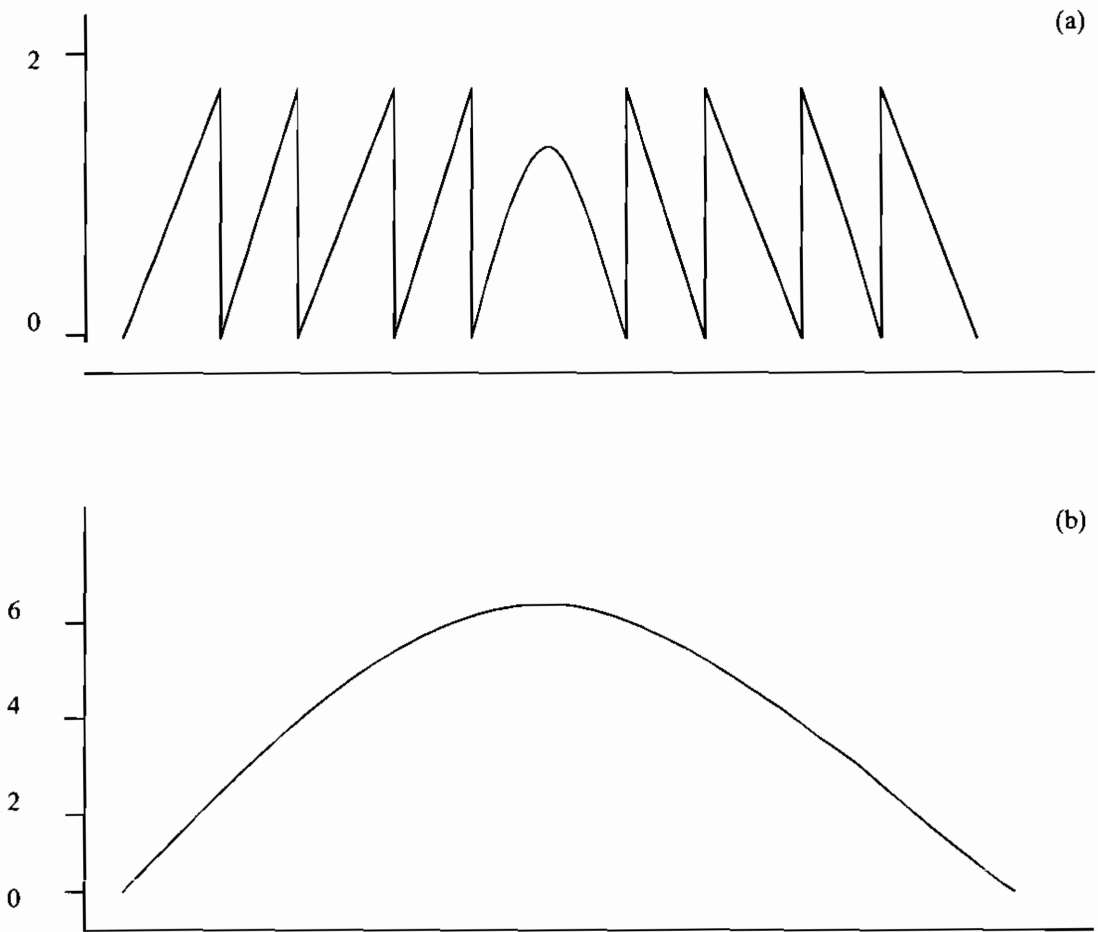

Fig. 2.14 (a) Characteristic saw-tooth "wrapped" phase function (b) Continuous function obtained by "unwrapping" the data in (a).

The key to reliable phase unwrapping is the ability to accurately detect the 2π phase jumps. In the case of noise free wrapped phase data and where this data is adequately sampled (i.e. the phase change between samples is significantly less than 2π) then a simple approach to phase unwrapping will be adequate. All that is required in this case is a sequential scan through the data, line by line, to integrate the phase by adding or subtracting 2π at the phase jumps.

In many measurement situations however, noise in the sampled data is the main contributing factor in the false identification of phase jumps. In this case as the amplitude of the noise approaches 2π, the real phase jumps become obscured. In the case of one-dimensional data, the only solution to this problem is to smooth the noisy sinusoidal fringe data with a low-pass filter. This is not entirely satisfactory since filtering always results in a loss of information.

For simple unwrapping methods to function satisfactorily, the data must be continuous across the whole image array and extend to the boundaries of the sample window. A phase discontinuity might be caused by a rapid change in the measurement parameter, such as a large height step in an object under test. This causes a sudden change in the fringe spacing or as a point where the fringe stops. In order to find methods for automatically detecting and dealing with such problems such as this sophisticated phase-unwrapping algorithms have been developed. Phase-unwrapping methods may be divided into path-dependant and path-independent methods.

Path-dependant methods are the simplest type and involve a sequential scan through the data, line by line. As can be see in Fig. 2.15 at the end of each line, the phase difference between the last pixel and the pixel on the line below is determined and the next line scanned in the reverse direction.

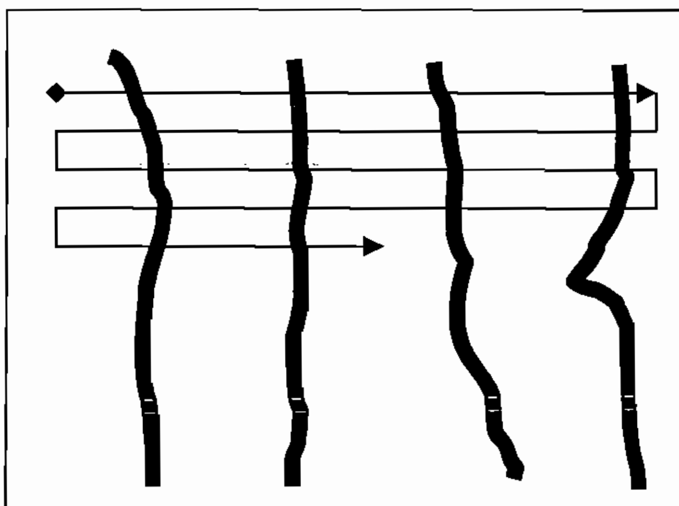

Fig. 2.15 Line by line sequential scanning path

This approach is effective when applied to high quality data, but more complex variations are necessary in the presence of noise. These include multiple scan directions, spiral scanning and counting around defects.

One of the most popular methods used to avoid phase errors propagating, is called pixel queueing. This involves unwrapping the regions of "good" pixel data first and then proceeding to the "bad" pixel data, thus confining data propagation errors to small regions.

Path-dependant phase unwrapping involves unwrapping the data by following all possible paths between any two points as opposed to unwrapping the data following a predefined path as in the path-dependant methods. An example of a path-independent method for phase-unwrapping was demonstrated by Ghiglia et al[14]. In a 3x3mm mask, the phase differences between the phase of the central pixel and each of its four nearest neighbours in the horizontal and vertical directions are calculated. If one of the differences is greater than 2π in absolute value, $+2\pi$ or -2π is added to the phase of the central pixel. Whether it is + or – depends on the majority of the 4 differences being positive or negative. When there are 2 positive and 2 negative differences, 2π is added. When none of the absolute differences exceeds π then the phase of the central pixel remains unchanged. This algorithm is very processing intensive, but also very immune to noise.

2.6 References

1. Hecht, E., Zajac, A., "Optics", 2nd ed., Addison-Wesley Publishing, 1987.
2. Dainty, J.C. (Ed.), "Laser Speckle and Related Phenomena" Topics in Applied Physics Vol. 9, Springer Verlag, Berlin, 1975.
3. Gasvik, K.J., "Optical Metrology", 2nd Edition John Wiley & Sons, 1995.
4. Jones, R., Wykes, C., "Holographic and Speckle Interferometry", Cambridge University Press, 2nd Edition, 1993.
5. Goodman, J.W: Chapter 2. "Laser Speckle and Related Phenomena" Dainty, J. C. (Ed.) Topics in Applied Physics Vol. 9, Springer Verlag, Berlin, 1975.
6. Butters, J.N., Leendertz, J.A., "Holographic and Video Techniques applied to Engineering Measurement", Transaction of the Institute of Measurement and Control, 1971.
7. Vest, C.M, "Holographic Interferometry", John Wiley & Sons, 1979.
8. Sirohi, R.S. (Ed.), "Speckle Metrology", Optical Engineering Series, Marcel Dekker Inc. Publishing, 1993.
9. Hung, Y.Y., Taylor, C.E., Proc. 7th South-eastern Conference on Theoretical and Applied Mechanics, 8,497, 1974.
10. Ganesan, A.R. et al, "Universal Digital Speckle Shearing Interferometer", Applied Optics, Vol. 27, No. 22, 15 Nov. 1988.

11. Ganesan, A.R., Sirohi, R.S., "New method of contouring using Digital Speckle Pattern Interferometry", SPIE Vol. 954 Optical Testing and Metrology 11, 327-332, 1988.

12. Stahl, H.P., "Review of Phase-Measuring Interferometry", Optical Testing and Metrology III: Recent Advances in Industrial Optical Inspection, Proc. SPIE Vol. 1332, Part 2, pp 704-719, 1990.

13. Robinson, D.W., Reid, G.T (Ed)., "Interferogram Analysis" IOP Publishing, Bristol, 1993.

14. Ghiglia, D.C., Romero, and L.A., "Robust 2-Dimensional weighted and unweighted Phase Unwrapping that uses Fast Transform and Iterative method", Journal of Optical Society of America: A, Vol. 11, Jan 1994.

15. Butters, J.N., Leendertz, J. A., "A double exposure technique for speckle pattern interferometry", Journal of Physics E: Scientific Instruments, 4, 277-279, 1971

Chapter 3.0 System design

3.1 Literature review

The first step in the design of the portable ESPI contouring system was an extensive literature review, in order to determine the techniques in use in the area to date. It was decided that the optimum features from each of the different techniques would be incorporated as much as possible, into the final system. These options are covered extensively in the following section.

3.2 Contouring Techniques

When deciding on the system design, each published method for ESPI contouring was carefully considered, and considerations such as budget, flexibility with respect to test objects and size were applied to each experimental component when making a decision on its suitability. The methods being considered were a) Spectral contouring and b) Angle of illumination change.

3.2.1 Spectral Contouring

In 1978, Jones and Wykes developed an ESPI system for measuring the difference between the shape of two surfaces [1]. A change in the relative phase between the two waves, object and reference, is introduced by changing the wavelength of the light between successive frames. The surface can also be illuminated simultaneously by a master wavefront at wavelengths λ_1 and λ_2 and the resultant speckle patterns are either added together or subtracted to produce the fringe pattern. For a range of sensitivities it is necessary to have a selection of wavelengths, and this is an important factor in the system design. To allow for this range of wavelengths, it is then necessary to have a tuneable wavelength source. With the budget consideration of the project, this might not have been a feasible method for the portable system. Tuneable laser diodes, with adequate output intensities are expensive and usually operate in the mid-infra-red region beyond the sensitivity of a CCD camera. It was decided to investigate this method in bench version as an opportunity arose during a visit to the European Commission Joint Research Centre in Italy in the early stages of the project, and this is detailed in section 3.3.1.

Using the same set-up, but immersing the object in a transparent liquid, a change in the refractive index of the liquid between two exposures induces a relative phase change in the interferometer related to the shape of the object surface. This method is obviously not suitable when flexibility with the type of test objects is taken into consideration.

3.2.2 Angle of illumination change

An alternative method for contouring a three-dimensional object was proposed by Ganesan and Sirohi in 1998 [2]. The method involves illuminating the object by two beams incident at equal angles on both sides of the optical axis. The object is rotated about an axis perpendicular to the plane containing the two illumination beams, producing a fringe pattern representing surface contour. Hertwig [3] proposed a similar method which involved rotating the illuminating beams as opposed to the object. Within the budget constraints of the project, both of these techniques were feasible.

It is important to compare the features of both and assess their suitability for the needs of the system. The next important issue is the size of the actual components which would bring about the rotation. Miniature rotation stages were found to be readily available but expensive in terms of the budget. A rotation stage for rotating the object (See Appendix A) was already available, but it would limit somewhat the type of object which could be examined due to size constraints. It was decided at this point, that of the two, the more expensive "rotate beams" method was superior in terms of object flexibility and the actual cost needed to be investigated.

Much time was spent in the sourcing of the miniature rotation stages commercially. It became clear that the prices were again out of the project budget, but that perhaps the

components could be purchased commercially and the stages constructed. It was decided that time spent in building the stages and testing their effectiveness would be worthwhile in the timeframe of the project. If the stages proved to be ineffective, then the "rotate object" method would become the method of choice.

A decision was made to incorporate both methods into the system design and to make a final decision at the end of the test procedure, on which method was the most effective.

3.3 Bench Prototypes

In the early stages of the project, it was necessary to build bench versions of the ESPI contouring systems from the literature, in order to become familiar with the set. The first method to be used was the spectral contouring method.

3.3.1 Spectral Contouring

This work took place at the European Commission Joint Research Centre (JRC) in Northern Italy. The mission of the JRC is to provide customer-driven scientific and technical support for the conception, development, implementation and monitoring of EU policies. As a service of the European Commission, the JRC functions as a reference centre of science and technology for the Union. Close to the policy-making process, it serves the common interest of the Member States, while being independent of special interests, private or national. To carry out its mission, the JRC has a unique combination of facilities and expertise transcending national boundaries. Moreover, through its networks it stimulates collaborative research and broadens its knowledge. The Centre for Industrial and Engineering Optics within the School of Physics, DIT has for some years now been involved in such collaborative research and joint ventures with the Institute for Systems, Informatics and Safety within the JRC and it is for this reason that the opportunity arose to visit and work there.

The bulk of the work conducted in Italy involved assisting in the development of the spectral ESPI contouring system. Its design is based on a Michelson interferometer and the object is illuminated with Titanium: Sapphire laser, which is pumped by an Argon Ion laser at a pumping power of 3.2W. The Ti:S starts lasing at a pumping power somewhere between 2 and 3W and it is possible to achieve an output of 700mW.

The system worked very well as an out-of-plane ESPI system, producing good quality fringes of high contrast. A birefringent filter in the cavity of the Ti:S laser was used to vary the wavelength in the range of 700-850nm making it suitable for contouring purposes. However, the fringe contrast diminished considerably when the system was used in this capacity and decorrelation was observed almost immediately after subtraction was started. The correlation length , i.e. the range within which the wavelength could be varied without causing decorrelation, was not even a couple of centimetres

The first objective of the work there was to assist in improving the contrast and more importantly, to discover why decorrelation was occurring so quickly i.e. with such a slight wavelength change (~0.05nm). An effective contouring system would need to have the capacity to vary the wavelength over a range of 10nm.

The bulk of the initial work with the system was optimising the set-up. This was achieved by using different optical configurations. Also, it was ensured that the optical path difference of the interferometer system was approximately equal to zero. The optimum wavelength operating range, in order to have approximately constant power for the various wavelengths, had already been established.

After a considerable length of time spent on this exercise, with little or no improvement in either the contrast or the correlation range, it was decided to insert an etalon into the Ti: S laser, in an attempt to increase coherence length. Two etalons of different

thicknesses accompanied the laser. The thinner etalon was inserted and after realigning the set-up, we obtained what appeared to be multiple fringe patterns, superimposed on one another, which moved independently of one another when the wavelength was varied. After much discussion it was proposed that these multiple fringe patterns were due to a number of different modes which arose due to the insertion of the etalon. At this stage, the time in the laboratory expired and so this problem was not solved during this visit.

At a later stage, some of the obstacles mentioned above were over come, but the method itself proved unsuitable for our purposes, due to the cost and low output intensity of tuneable laser diodes. The important aspects of portability and size, in the design of the system could not be catered for when utilising this method. Despite the latter's' obvious advantage of no moving parts, the angle of illumination methods were deemed to be more suitable.

3.3.2 Angle of Illumination change

A single good quality rotation stage suitable for rotating test objects was available. Therefore it was appropriate to first build the "rotate object " type of system. The system proved to work successfully, producing fringe patterns that were consistent with the

object shape. The single disadvantage to this method seemed to be the limiting factor with respect to the size and shape of the object. If the object were too large or heavy, then the rotation stage would not be capable of supporting it. If the object did not have a flat base, then problems would continuously arise during the mounting procedure, though this would be the most easily overcome of the two. Since this method proved successful during the preliminary test period and produced satisfactory fringe patterns it was decided to concentrate on the miniature rotation stage building, and thus compare and prioritise the advantages and disadvantages of this "rotate object" method once the "rotate beams" method had been tested also.

3.4 Miniature Rotation Stages

As outlined previously, in order to obtain more flexibility with the objects which could be examined using the contouring system, it was necessary to build miniature rotation stages to change the angle of illumination. It was decided that at this point to purchase miniature stepper motors together with gearboxes to match the resolution to those commercially available. A suitable stepper motor driver board would also be purchased and the rotation stages would be custom built and would be controlled by LabVIEW©. This task was undertaken successfully, and a list of components is included in the Appendix A.

3.4.1 LabVIEW© software

LabVIEW© is a highly productive graphical programming environment that combines user friendly graphical development with the flexibility of a powerful programming language. It is used particularly in the fields of engineering and science for data acquisition, data analysis and data presentation. It features built-in compatibility with hardware libraries for motion control and image acquisition, making it suitable for the simultaneous control of the rotation stages and the imaging, subtraction and rectification processes. The software for control of the system has a graphical user interface which can be seen in Fig. 3.1.

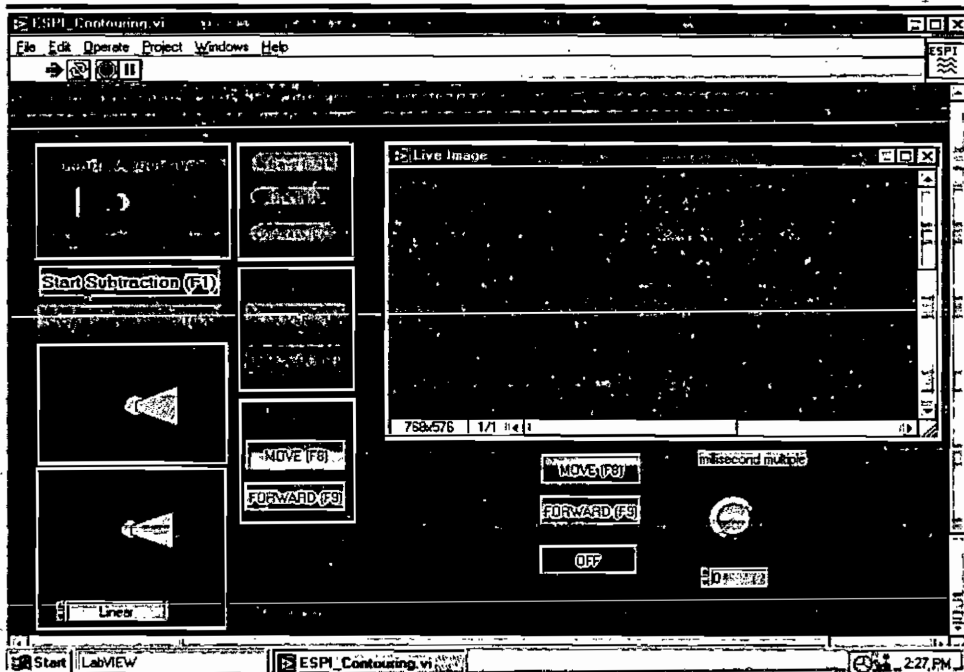

Fig. 3.1 LabVIEW© user interface for the ESPI contouring software

The software includes filtering and pixel intensity stretch functions in addition to the basic functions of controlling the motors and image acquisition. At this point, the software did not allow for phase mapping or unwrapping. It was decided to determine the effectiveness of the miniature rotation stages in terms of fringe contrast, before investing more time in the phase analysis capabilities of the software.

3.5 Building the system

3.5.1 System layout

The system was built using Spindler & Hoyer (See Appendix A) microbench and optics, with an Etteymeyer GmbH laser diode (See Appendix A). The diode would allow for frequency modulation phase shifting once the system's contrast was sufficiently high. According to the final system design, the layout was to be as in Fig. 3.2.

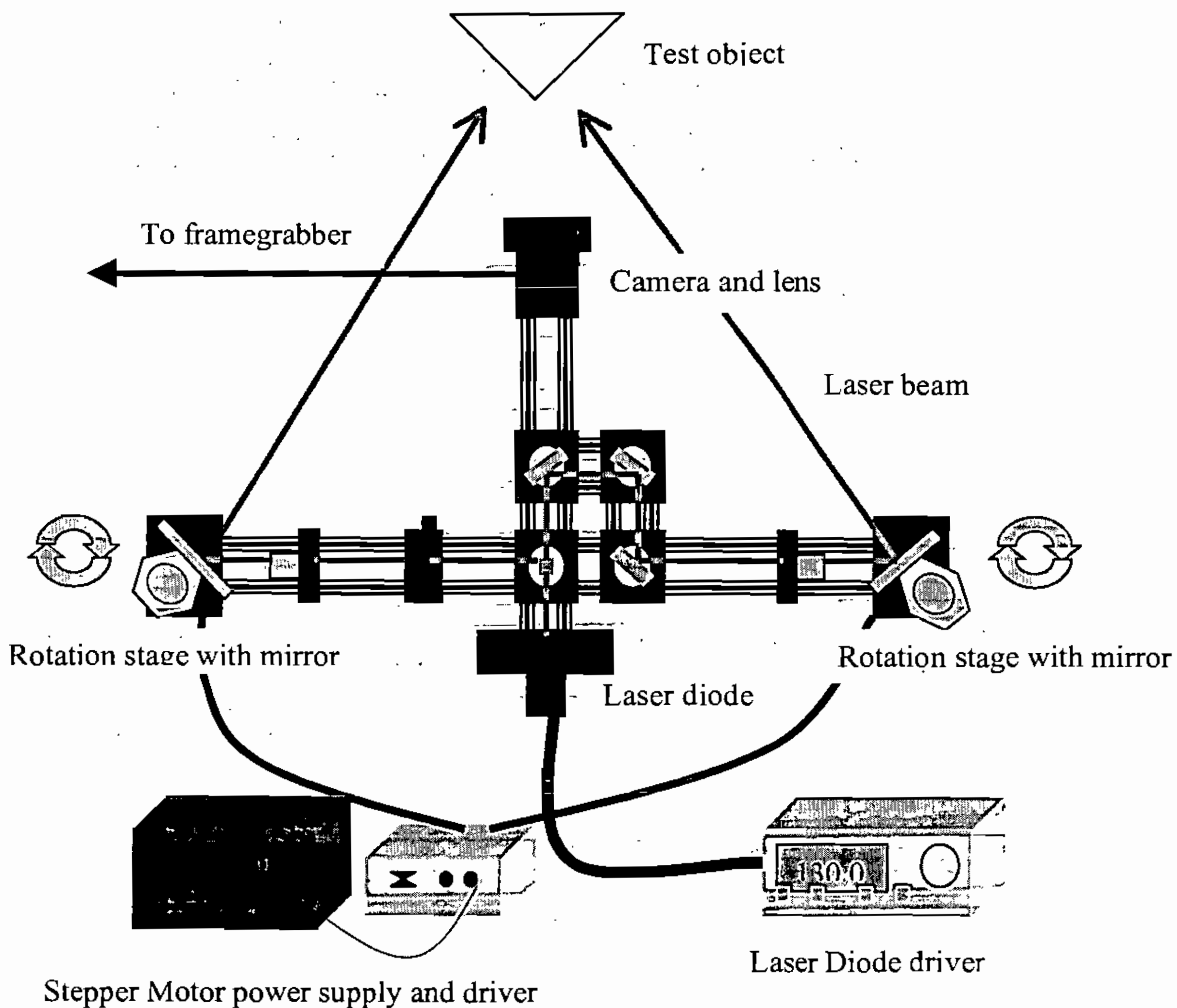

Fig. 3.2 ESPI contouring system as designed and built within the project

The diode has a wavelength of 785nm and its beam enters a beamsplitter. One half of the beam travels straight to one of the illuminating mirrors on the left-hand side of the diagram. The other half travels through a series of three mirrors before arriving at the illuminating mirror on the right-hand side of the diagram. This is necessary so as to

introduce a path-length difference between the two beams for the purposes of frequency modulation phase shifting. This will be explained in more detail in section 3.5.2. The illuminating mirrors are mounted on the custom-built rotation stages which have a resolution of 0.0018°. It is possible to adjust the angle at which the mirrors are mounted manually, as well as rotating them on the stages.

The entire system is mounted on a duralium beam, which was specifically cut and drilled for the purpose. The material is similar to the material of the Spindler and Hoyer microbench and is both strong and lightweight. It is attached to the system at the base of each of the two motors. The beam has a dual purpose: 1) to add stability to the system and 2) to allow the system to be bolted onto a tripod for height adjustment and portability. The beam also allows the system to be bolted onto a laboratory optical bench which further stabilises it for testing.

The commercial Oriel Encoder Mike Controller Rotation stage (see Appendix A) is added to the laboratory set-up for the purposes of rotating the object. The driver box is located away from the optical bench so as to avoid any contact with the test set-up. The object to be examined is placed on the rotation stage and so can be tested using both techniques without adjustment to the set-up. Fig. 3.3 shows a photograph of the system.

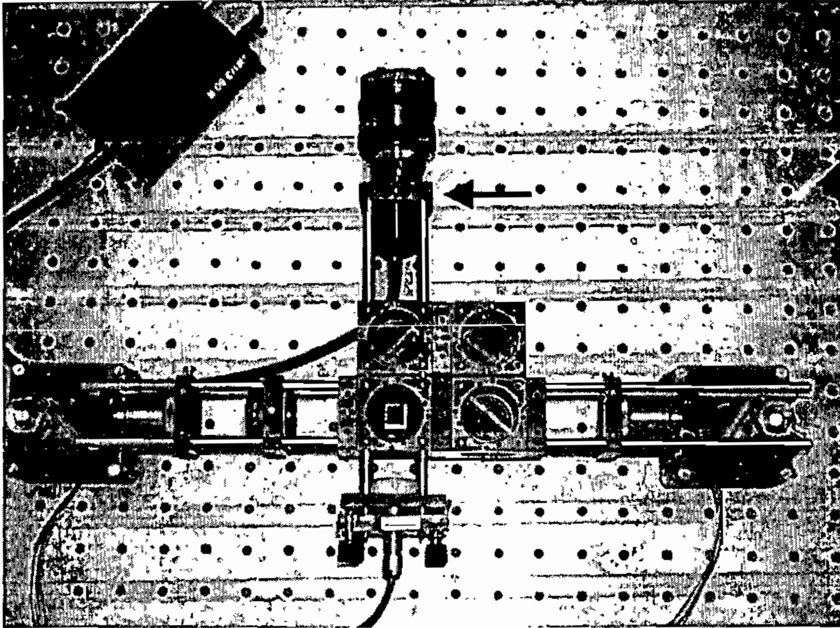

Fig. 3.3 The final system

The system measures 44-cm x 25-cm x 12-cm. The miniature CCD camera indicated in the photograph is supplied by Spindler and Hoyer and its technical specifications are given in Appendix A. The LabVIEW© software discussed in the previous section is used to control the system when the "rotate beams" method is used. As stated previously, the package has not yet had the phase shifting capabilities incorporated into it. However, when using the "rotate object" method, which does not require computer control for the rotation, it is possible to use existing completed software developed at the Joint Research Centre for the image acquisition etc. The software is called ESPITest© and the following section describes it in detail.

3.5.2 ESPITest software

ESPITest can be used to control any interferometry system that uses low-voltage phase shifting devices, a standard CCD camera and a framegrabber. The package is Windows NT based and is equipped for acquisition, control and post-processing for electronic speckle pattern interferometry.

The program consists of smaller sub-programs which are each responsible for a particular task. One of these communicates with the framegrabber for example. When the program is started, a tool bar at the top of the screen allows the user to click on a particular icon to view its sub-program menus. The two main icons are "Calibrations and Settings" and "Vidco Acquisition. The former contains all the controls necessary for the calibration and settings of the various measurement devices, including the framegrabber and the analogue output board. It also contains a median filter setting. The "Video Acquisition" menu contains the controls for image acquisition, ESPI subtraction, and wrapped phase map calculation. Fig. 3.4 shows the user interface and the sub-programs previously mentioned.

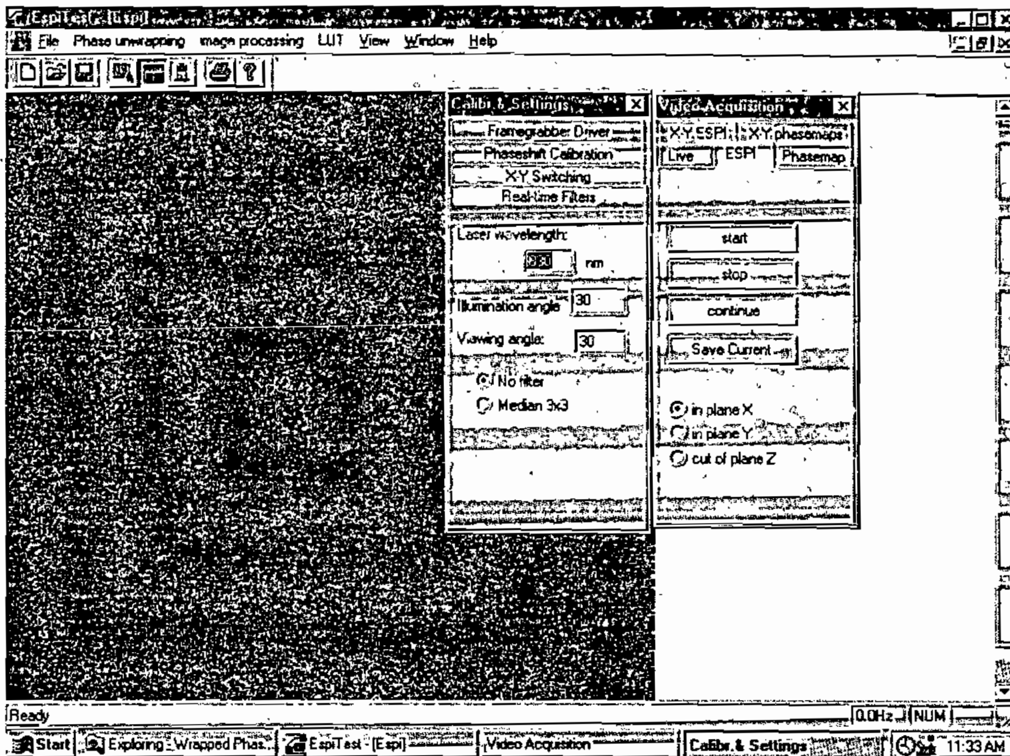

Fig. 3.4 User interface for the ESPITest software

A Data Translation framegrabber board is used to acquire and digitise the analogue signals from the CCD camera. The software performs subtraction and rectification and displays the subsequent fringe pattern on the monitor. When phase shifting has been incorporated into the system, the software uses the phase shifting algorithm described in Chapter 2 to calculate the wrapped phase maps. It then uses an unwrapping algorithm to unwrap this data and convert it to profile data.

A National Instruments D/A board is used to control the phase shifting by modulating the current being supplied to the laser driver. This results in a small modulation in the laser frequency and hence a phase shift between the two illuminating beams, which have unequal path lengths. The technique is known as frequency modulated phase shifting [4]. The software is capable of calibrating this phase shift while an image of the surface illuminated by the two beams is being acquired.

Each pixel in the image will modulate in a sinusoidal way as the phase changes between the illuminating beams. The ESPITest software records the intensities of 16 pixels in the image and plots the intensities as a function of the applied voltage. If the device has a linear response, the plotted intensities should have a sinusoidal shape. A sine wave is fitted to the data so that the voltage corresponding to a phase change of 2π can be obtained. When this voltage has been determined, it is divided by four to calculate the voltage required to change the phase by $\pi/4$.

Only some of the pixels will modulate in the predicted manner. Since the images are inherently noisy, the software ignores the four worst-fit data plots. It then weights the other 12 according to how closely each signal represents a sine wave. If the user does not agree with the calculated voltage, then red and green vertical cursors can be used to select a new voltage.

At this point, the system is ready for phase map operation. It does this by taking four images as it shifts the phase by 0, $\pi/2$, π, and $3\pi/2$. It uses these images to work out the subsequent phase change caused by rotation of the object and displays the data as wrapped phase fringes. It is possible to unwrap these fringes to produce a high-resolution phase map and then the surface height map.

If it is only necessary to obtain qualitative data, then the system can be used in "ESPI" mode to simply produce contour fringe patterns.

3.6 Comparison of the two methods

3.6.1 "Rotate Beams" method

At this point, the system had been built to the design specifications decided upon in the previous sections. The experimental layout was such that both the "rotate beams" and "rotate object" methods could both be used. The miniature rotation stages were causing concern at this point due to excessive vibration and an audible noise during operation. It was feared that these would result in fringe contrast too low for phase shifting analysis to be performed.

Initially, the system was tested with a variety of different objects. The first results obtained were contouring fringes of a cylindrical plastic pipe. The fringe pattern was as expected but the contrast quality was very low. Since the plastic pipe is a volume scatterer, which gives faster decorrelation than surface scatterers, this explains somewhat the poor contrast. An example of a fringe pattern from this first series of results can be seen in Fig. 3.5.

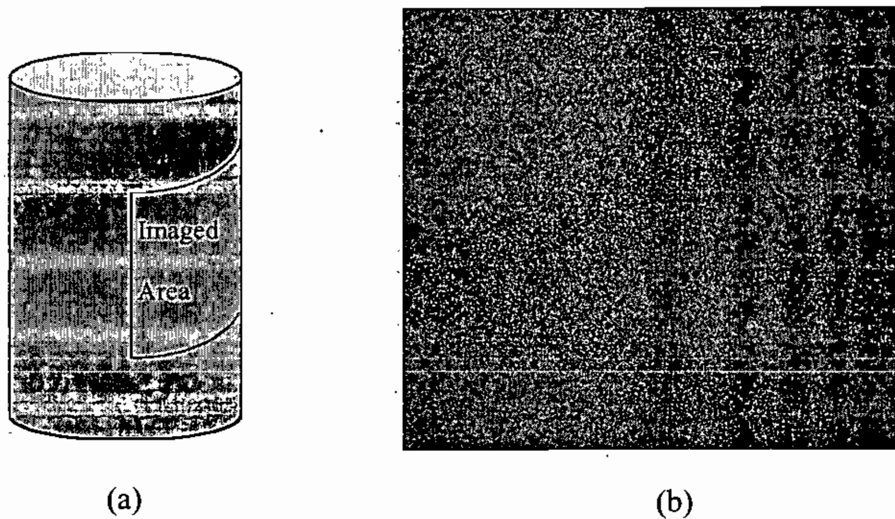

Fig. 3.5-(a) schematic showing test area. (b) Fringe pattern from area indicated in (a)

The object, i.e. a cylinder is viewed at one side, with its centre positioned on the left-hand side of the above fringe pattern.

It could be observed while the system was operating that the poor contrast could also be somewhat attributed to the vibration of the motors, since it improved slightly when the

motors were stopped. However, several attempts to stabilise the system by fixing it more formally to the optical bench, checking the components for stability and securing the mirrors, did not improve the contrast in any way.

At this point the duralium beam was added to the system in an effort to stabilise the motors at the base and perhaps reduce the vibration. The beam was also to be used as a baseplate for attaching the system to a tripod for portability. This however, did nothing to alleviate the problem of poor contrast.

The reason for this poor contrast is clear when it is considered how decorrelation occurs in ESPI. Speckle Interferometry measures the change in intensity between two speckle patterns. It does this by imaging each speckle onto an element of a detector array and measuring the change in intensity of the light at that element. The light must come from the same speckle in most cases. If the speckle is displaced such that the light incident on the pixel now comes from a different speckle, there will be no correlation between the two intensities. This will inevitably lead to decorrelation.

Decorrelation begins as soon as the surface starts to be displaced or the beams start to move, depending on the type of ESPI. However, the effect is insignificant initially, since the displacement or rotation is so small, that the speckle movement is very small relative to the size of the speckles. If each speckle on the object is imaged onto just one pixel, and the object moves by the size of a speckle, total decorrelation will occur.

Vibration is one of the major causes of decorrelation in ESPI. If the speckles are moving as the frame is grabbed, it has the effect of averaging the fringes and so reducing the contrast. For this reason, an ideal ESPI system will have no moving parts. The vibration of the system under test in this project is causing the poor fringe contrast due to decorrelation as just described. Since none of the methods attempted to alleviate the problem proved to be successful, the second method, "rotate object" was tested for its level of contrast and suitability for phase shifting analysis.

3.6.2 "Rotate Object" Method

The system was tested on the same surface, the cylindrical pipe, in the same experimental set-up. An immediate improvement was noted in the fringe contrast despite the presence of a moving part in the set-up i.e. the rotation stage on which the object was placed. The difference in this situation was the absence of vibration which was the reason for the poor contrast in the "rotate beams" method.

Fig. 3.6 shows an example of the first results obtained using this method. The contrast is significantly better than that achieved with the previous method.

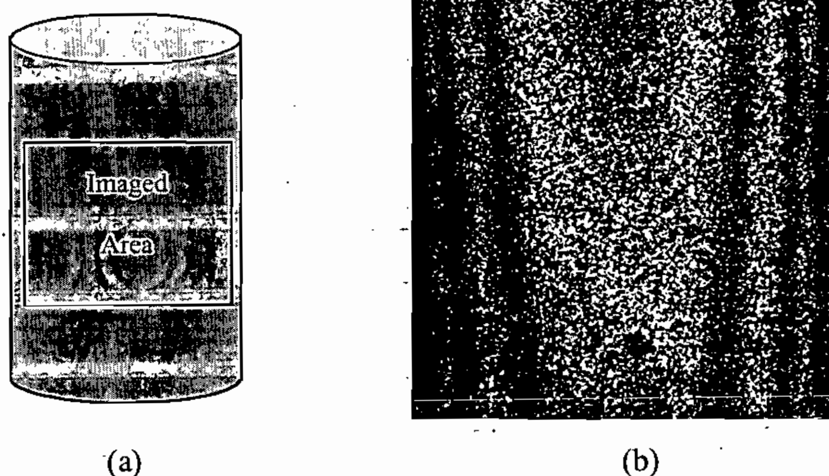

(a) (b)

Fig. 3.5 Fringe pattern obtained using the "rotate object" method.

It was decided that the "rotate object" method was by far the superior of the two in terms of contrast. For phase shifting analysis it is imperative that the speckles are perfectly still and so the vibration of the motors used to rotate the beams in the first method make it unsuitable for the purposes of the project. Whilst the "rotate object" method does involve a moving part, and therefore will exhibit decorrelation and poor contrast when compared with in-plane or out of plane ESPI, its contrast is still superior to the "rotate beams" method, since the vibration factor has been removed

The following chapters present the results obtained with the system using the "rotate object" method. Chapter 4 contains results obtained through the fringe counting technique described in Chapter 2. Chapter 5 contains the results obtained through phase shifting analysis, also described in Chapter 2.

3.7 References

1. Jones, R., Wykes, C., "Holographic and Speckle Interferometry", Cambridge University Press, 2nd Edition, 1993.
2. Sirohi, R.S. (Ed.), "Speckle Metrology", Optical Engineering Series, Marcel Dekker Inc. Publishing, 1993.
3. Hertwig, M., "Application of Improved Speckle Contouring Technique to Surface Roughness Measurements", Optics and Lasers in Engineering 26, 115-130, 1997.
4. Onodera, R., Ishii, Y., "Frame rate phase-shifting Interferometer with a Frequency-Modulated laser diode", Optical Engineering 38(12), 2045-2049, 1999.

Chapter 4.0 Results with Fringe Counting analysis

4.1. Introduction

A fringe pattern produced by the system described in Chapter 3, represents the surface contour of the particular object being examined. In order to obtain from this fringe pattern the quantitative data necessary to reconstruct the surface profile, certain experimental conditions need to be recorded along with the patterns

Firstly, it is imperative that the area which is being imaged by the CCD camera is measured and recorded. To do this, a scale is placed across the object surface and viewed on the live image in ESPITest (See Appendix B) as in figure 4.1 below.

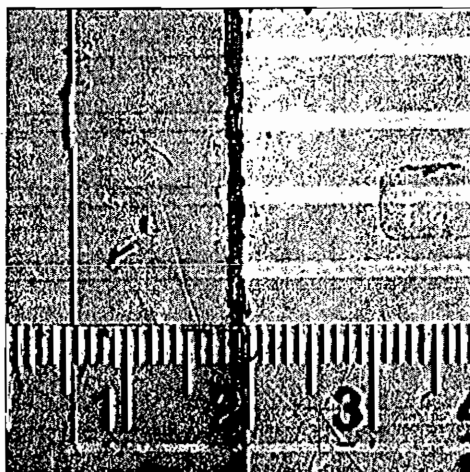

Fig. 4.1 Live view of a cube edge with scale.

In this example it can be seen from the scale that the area imaged by the camera is approximately 38mm square, represented by 512 x 512 pixels. The number of fringes we can expect to see depends on the system sensitivity. As discussed also in Chapter 3, this depends on two system parameters. Firstly the sensitivity depends on ϑ the illuminating angle and secondly on $d\vartheta$ the amount of rotation which has taken place. It is also important to note fringe order as the pattern develops. At this point, a thorough analysis of some simple objects i.e. a cube edge and a cylinder will be undertaken using this fringe counting method. The contour patterns will be produced by rotating the object, as decided upon in the previous chapter, "System design".

4.2 Fringe Counting analysis of a Cube edge

In this first series of results i.e where the cube mentioned previously is the object and the live image from Fig. 4.1 represents the area being imaged, ϑ is 12.5° and the value of $d\vartheta$ was progressively increased by means of the Oriel Encoder Mike Controlled Rotation Stage (see Appendix A-Equipment). As this angle $d\vartheta$ increases so too does the number of fringes across the object surface. A schematic of the object's position with respect to the camera and the actual area being imaged is shown in Fig. 4.2 on the following page.

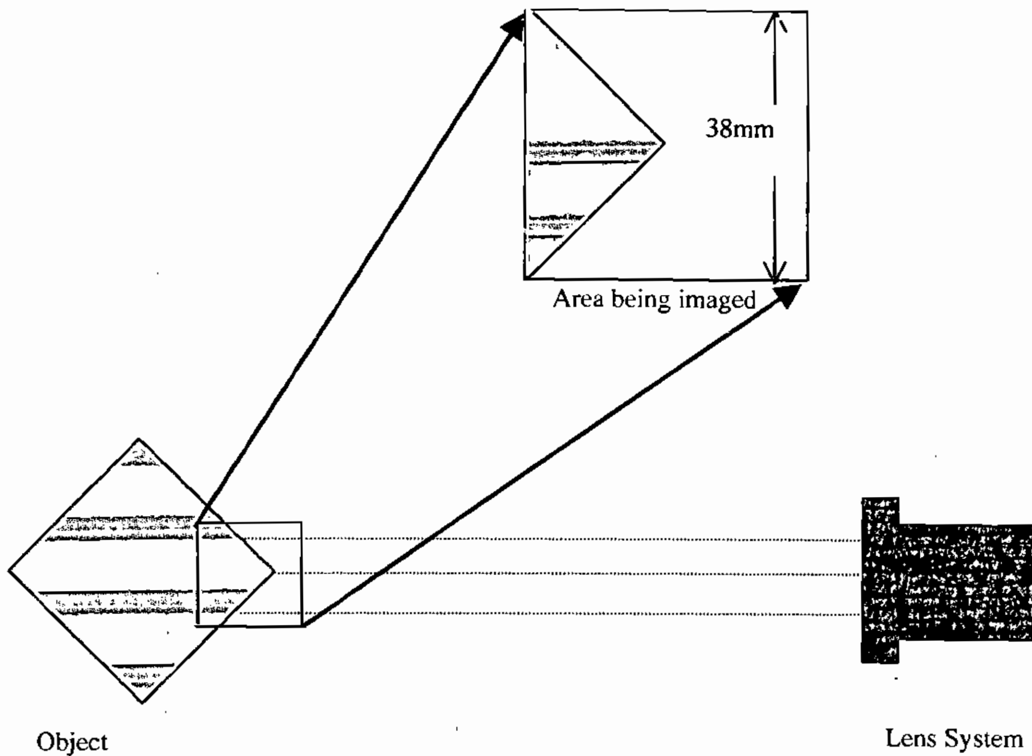

Fig. 4.2 Schematic of the area being imaged for the analysis of a simple cube shape

The meaning of fringe spacing has also been dealt with in Chapter 2, and so only the equation will be given here:

$$\Delta z = \frac{\lambda}{2 Sin\,\vartheta Sin\,\delta\vartheta}$$

where λ is the wavelength of the illuminating source and the other symbols are as before. For this series of results, the wavelength of the laser diode is 785nm. An aerial

view of the whole optical set-up can be seen in Fig. 4.3 below. As can be seen from the diagram, the set-up allows for the object to rotate to produce the contour fringe patterns.

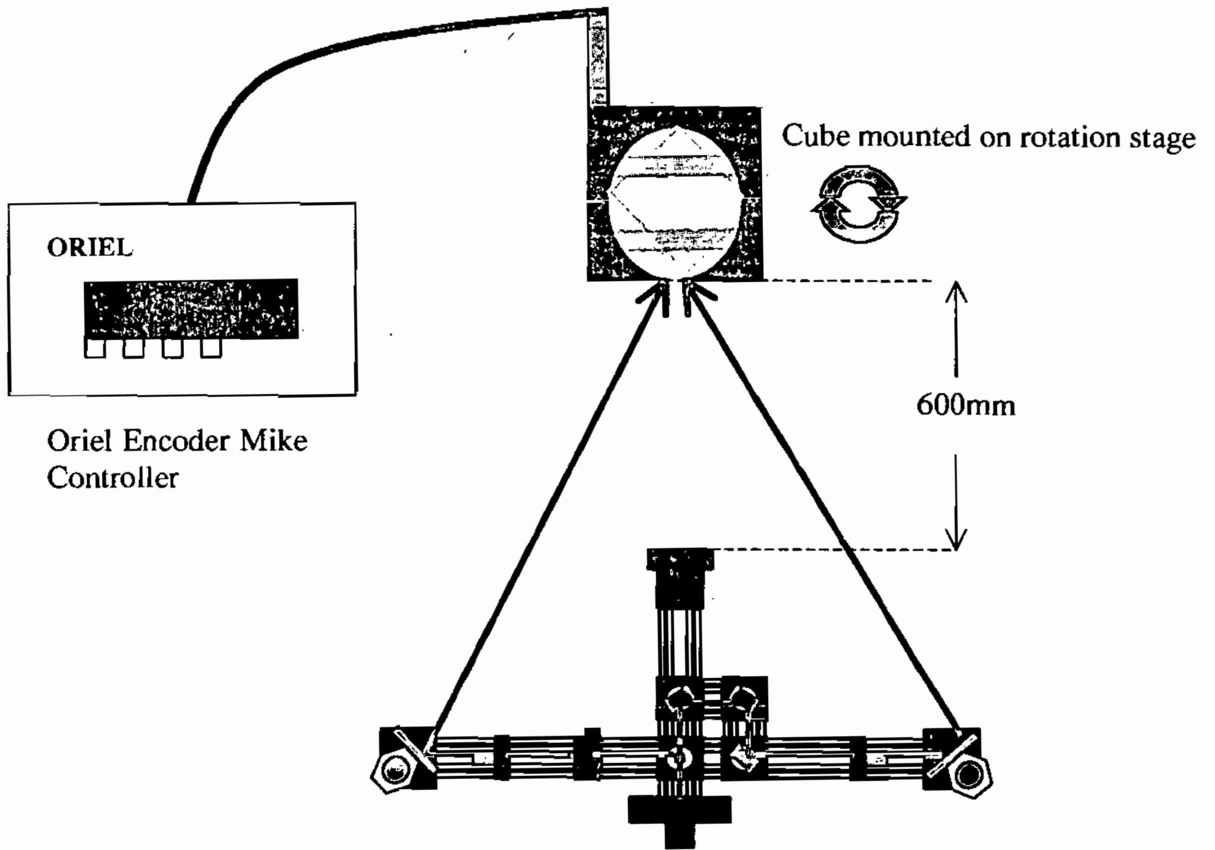

Fig. 4.3 Optical set-up for first series of results. Object is a cube viewed at one edge

4.2.1 Rotate Object in clockwise direction

The actual values of dϑ for the clockwise experimental series were 0.0062°, 0.0093°, 0.0124°, 0.0155° , 0.0186° and 0.0217° respectively. These angular values correspond to increments of 0.5 of the arbitrary units which the rotation stage uses. The set of fringe patterns corresponding to the above series can be seen in Fig. 4.4 below.

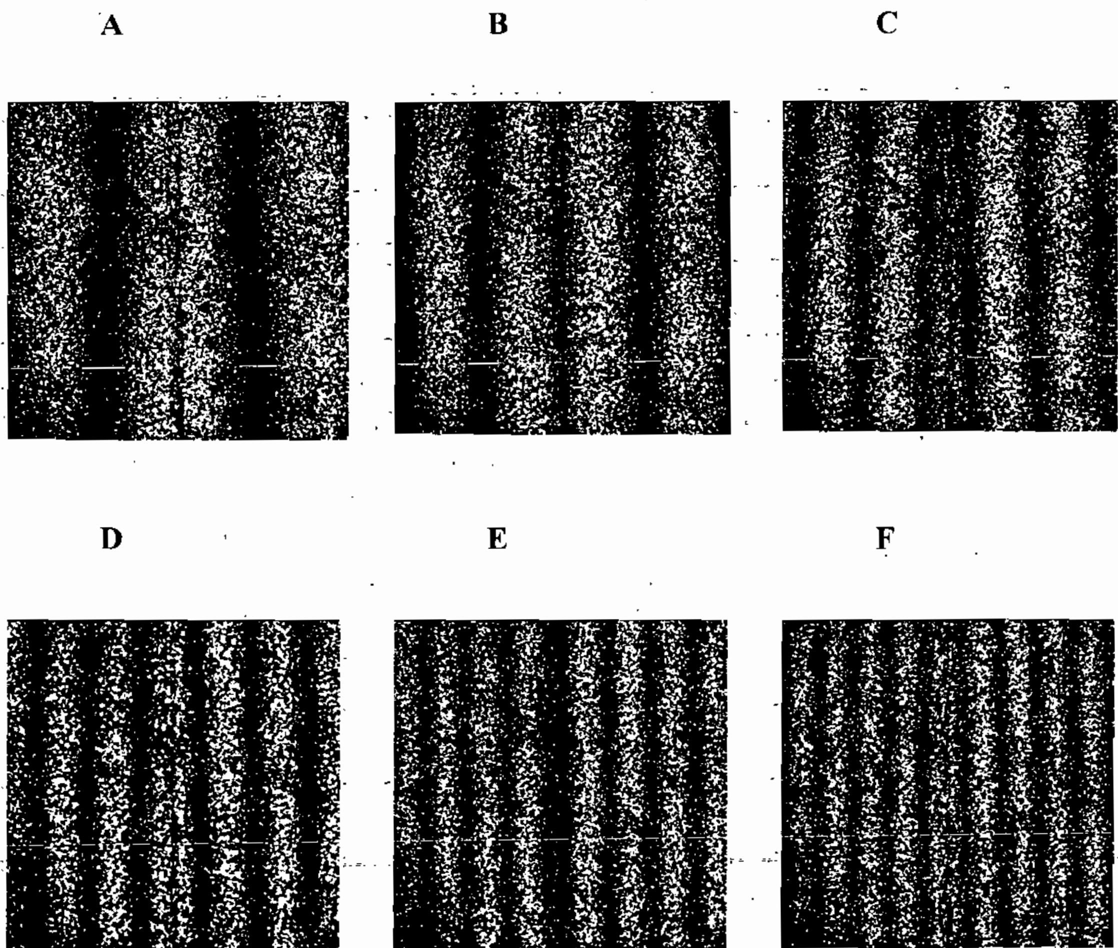

Fig. 4.4 Fringe patterns corresponding to rotations of:. A= 0.0062 °, B= 0.0093 °, C= 0.0124 °, D= 0.0155 °, E= 0.0186 °and F= 0.0217 °

As an example, one fringe pattern was chosen i.e. with $d\vartheta = 0.0155°$. This gives a Δz value of 6.7mm. The fringe pattern was opened in an image processing package called Scion Image (See Appendix B). Within this package, it was possible to set a millimetre per pixel scale and hence assign x-axis positions to the fringes as can be seen in Fig. 4.5.

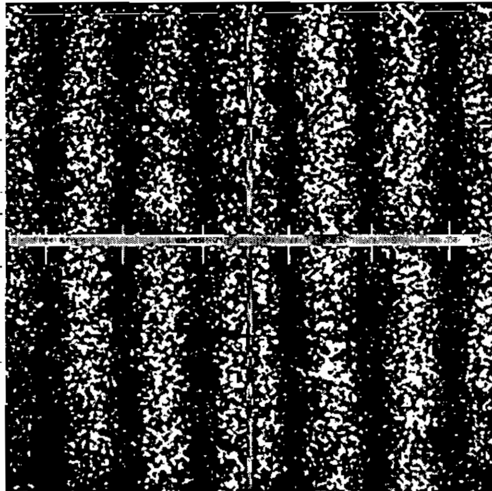

Order: 1 2 3 3 2 1

Fig. 4.5 Fringe pattern with fringe positions marked off and order number assigned

Cube edge, $d\vartheta = 0.0155°$, $\Delta z = 6.7mm$

Fringe order number, as stated earlier is noted whilst the pattern is developing. Since the fringes appear from the cube edge which is approximately at the centre of the image in this example ie the 19mm mark on the horizontal axis (see red line), then the fringe nearest to the cube edge is assigned the highest order number as it has appeared most recently.

The order number for each fringe is multiplied by the Δz value, 6.7mm to give the z-axis values corresponding to the x-axis fringe positions, seeTable 4-A:

TABLE 4-A

X-Axis Position/mm	Fringe Order No.	Z-Axis Position/mm
3.01	1	6.7 (6.7 x 1)
9.05	2	13.4 (6.7 x 2)
15.21	3	20.1 (6.7 x 3)
21.5	3	20.1 (6.7 x 3)
28.2	2	13.4 (6.7 x 2)
34.5	1	6.7 (6.7 x 1)

Table 4-A: X- and Z-Axis position / mm with corresponding fringe order number for a cube viewed at one edge with a clockwise rotation of 0.0155°

From this data, it is possible to produce a graph which illustrates the surface profile of the object, by plotting the difference in depth between adjacent fringes, Δz versus the x-axis position of the fringes. This is illustrated in Fig. 4.6.

Fringe Pattern

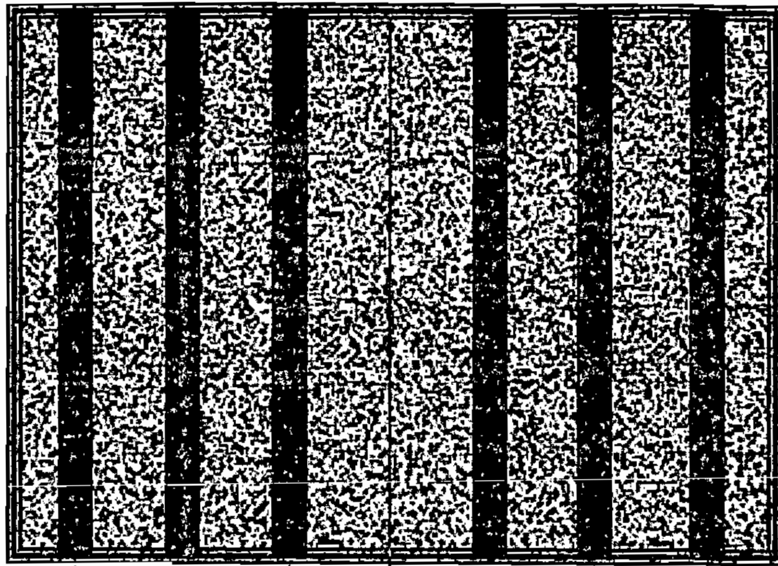

Ariel view of Δz

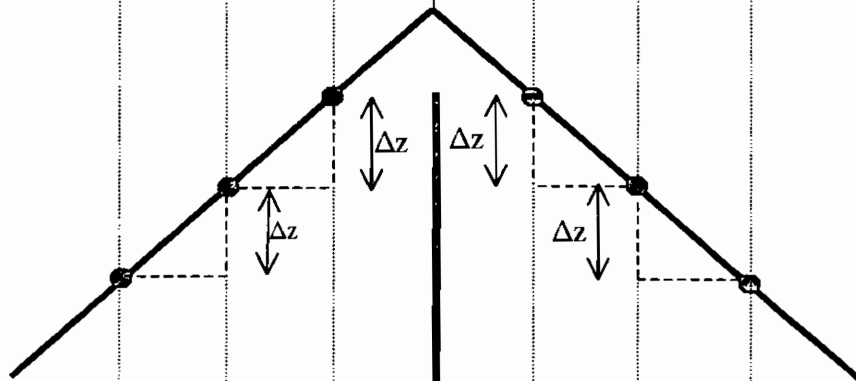

3-D Cube fringe positions

Z-axis Position

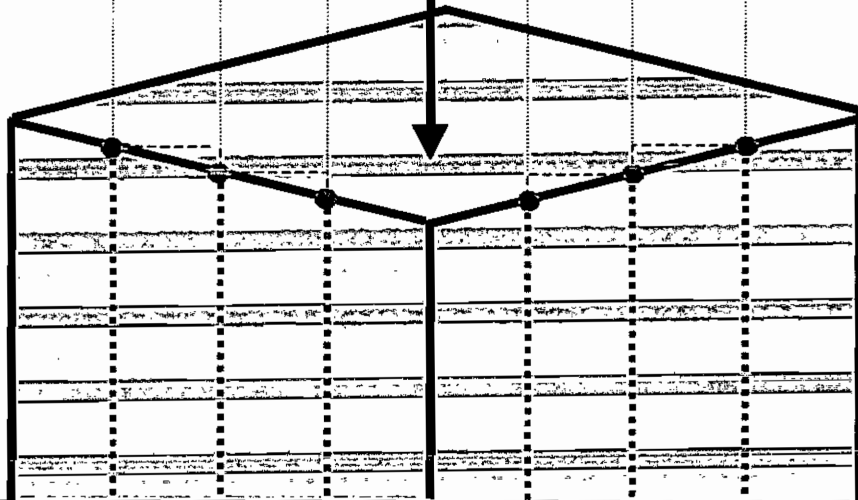

0 X- axis Position 38

Fig. 4.6 Diagram of relationship between fringe pattern and Δz values

Since in this case the object is the edge of a cube, it is safe to assume that a graph displaying a set of points for each side of the cube, whose best fit lines meet at a 90°

angle will show the system to be effective. Such a graph is shown in Fig. 4.7 and the product of the slopes of the best fit lines is -1 proving that the 90° angle has been constructed.

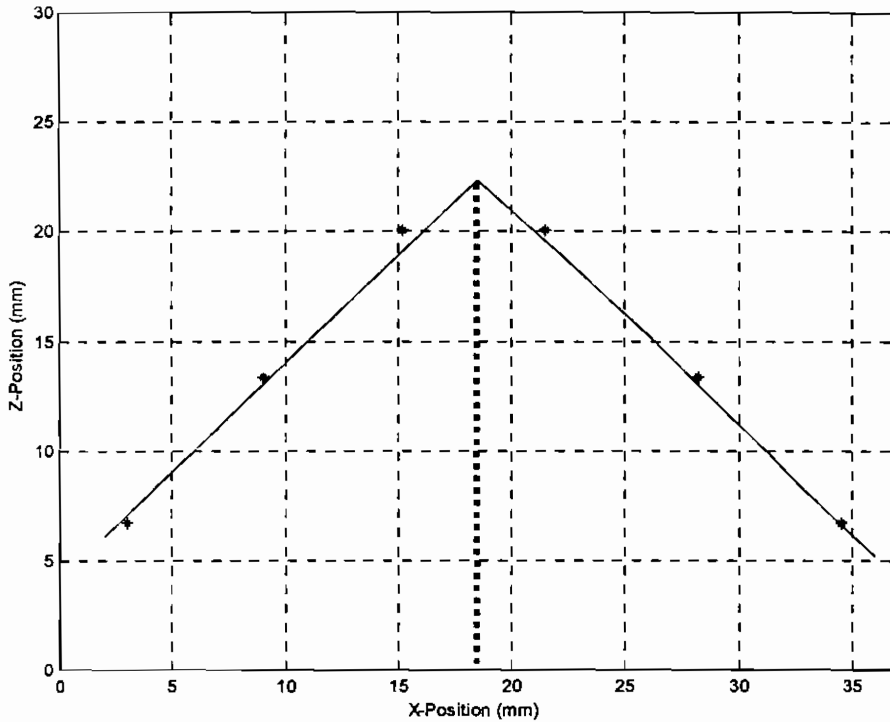

Fig. 4.7 Surface profile of a cube edge.

Cube edge, $d\vartheta = 0.0155°$, clockwise, $\Delta z = 6.7mm$

As can be seen from this graph (Fig. 4.7), the position of the edge of the cube is determined by extrapolation of the best-fit lines to be approximately 18.5 mm. From Fig. 4.1 we can see that this agrees with the measurement taken from the scale of between 18-19mm. This shows that not only is the system producing the correct profile but that with respect to the image view of the camera, the spatial information which the graph produces is in agreement with the physical set-up.

Fig. 4.7 represents the fringe pattern in Fig. 4.5, a pattern which contains 6 fringes. In a further test, a fringe pattern (Fig. 4.8) with 8 fringes and a $d\vartheta$ value of 0.02177° was chosen. The value of ϑ is again 12.5°. The value of Δz for this fringe pattern was found to be 4.8mm.

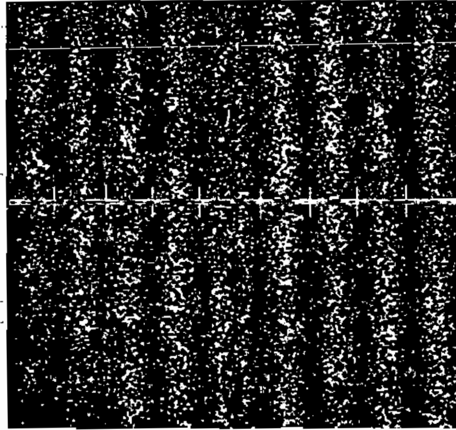

Order: 1 2 3 4 4 3 2 1

Fig. 4.8 Fringe pattern with fringe positions marked off and order number assigned

Cube edge, $d\vartheta = 0.02177°$, $\Delta z = 4.8$ mm

As in the previous example, the x- and z-axis co-ordinates are determined and the values in this instance can be seen in Table 4-B.

TABLE 4-B

X-Axis Position/mm	Fringe Order No.	Z-Axis Position/mm
2.50	1	4.8
7.01	2	9.6
10.99	3	14.4
16.25	4	19.2
21.23	4	19.2
26.91	3	14.4
31.5	2	9.6
37.5	1	4.8

Table 4-B: X- and Z-Axis position / mm with corresponding fringe order number for a cube viewed at one edge with a clockwise rotation of 0.02177 °

Using the values from the above table, the graph in Fig. 4.9 was produced. Again, the angle made by the best-fit lines is approximately 90° and the product of the slopes of the best fit lines which represent the sides is -1, showing the system and method of analysis to be effective with the cube edge again extrapolated to between 18-19mm.

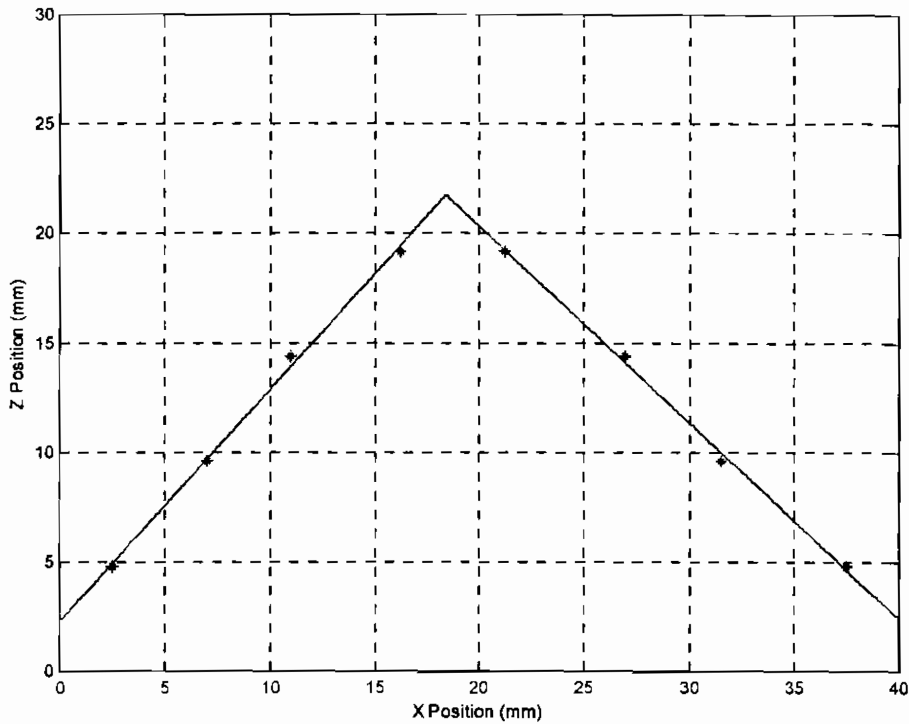

Fig. 4.9 Surface profile of a cube edge

Cube edge, $d\vartheta = 0.02177°$, clockwise, $\Delta z = 4.8$ mm

With this set of results, the system has been proved to be an effective in producing a profile of a simple shape. This section of this analysis has tested a simple shape by rotation in the clockwise direction. In order to ensure that the system is indeed producing valid results, it is necessary to test for rotation in the anticlockwise direction also. The following section deals with this comparison.

4.2.2 Rotate Object in the anti-clockwise direction

The next step in the analysis is a test of the direction of rotation on the effectiveness of the system. In this instance, the same series of results is repeated with $d\vartheta$ taken in the anticlockwise direction as opposed to the clockwise direction from the previous section. A fringe pattern with 8 fringes suitable for analysis was chosen, with a $d\vartheta$ value of 0.01866° giving a Δz value of 5.6mm. As before, the fringe pattern in Fig. 4.10 was analysed using the Scion Image package.

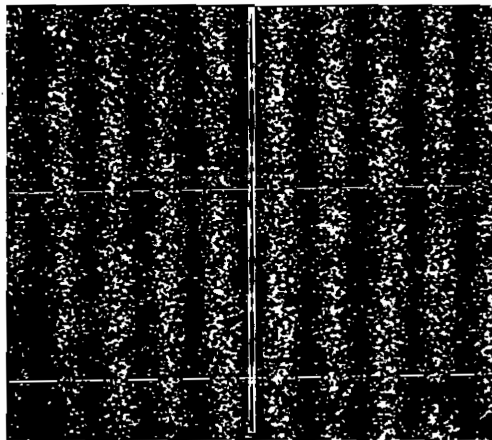

Order: 1 2 3 4 4 3 2 1

Fig. 4.10 Fringe pattern with fringe positions marked off and order number assigned

Cube edge, $d\vartheta$ = 0.01866°, Δz = 5.6 mm

The values for x- and z-axis position and fringe order can be seen in Table 4-C.

TABLE 4-C

X-Axis Position/mm	Fringe Order No.	Z-Axis Position/mm
0.91	1	5.6
5.13	2	11.2
9.80	3	16.8
15.73	4	22.4
22.04	4	22.4
28.99	3	16.8
35.54	2	11.2
38.00	1	5.6

Table 4-C: X- and Z-Axis position / mm with corresponding fringe order number for a cube viewed at one edge with an anti-clockwise rotation of 0.01866 °

As in the case of clockwise rotation in the previous section, plotting of this quantitative data retrieved from the fringe pattern produces a graph representing two sides of the cube object under evaluation. Again, these two sides are represented by the data on Fig. 4.11. The best-fit lines meet at an angle of approximately 90°, with the product of the slopes of each side being -1, proving that the system works just as effectively while being rotated in the anticlockwise direction.

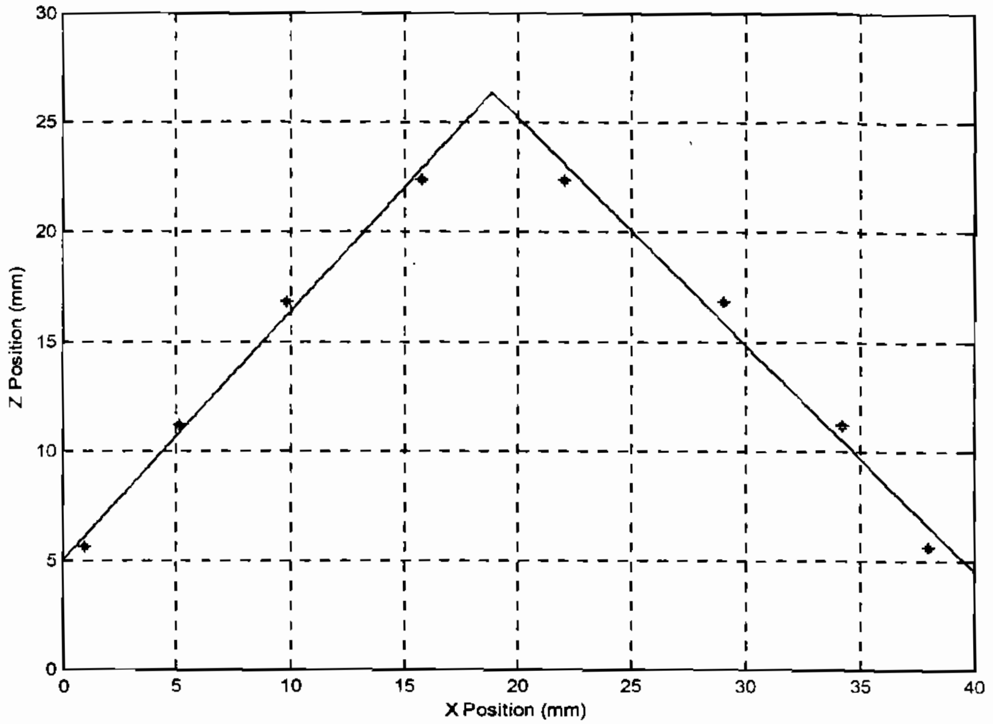

Fig. 4.11 Surface profile of a cube edge

Cube edge, $d\vartheta = 0.01866°$, anticlockwise, $\Delta z = 5.6$ mm

Also, as in the previous examples for clockwise rotation, the graph is extrapolated to determine the position of the cube edge along the horizontal or x-axis to be between 18-19mm, which again, in in agreement with the actual measurements taken of the experimental set-up.

The system has been proven to work effectively using fringe-counting analysis. The following section describes the same analysis on another simple shape i.e. a cylindrical pipe.

4.3 Fringe Counting Analysis of a Cylinder

In this second series of results, the object under examination is a cylinder, a live image of which can be seen in Fig. 4.12 below. As before, the area being imaged is 37mm squared, represented by 512 by 512 pixels. In this case ϑ is 14.4° and the value of $d\vartheta$ was progressively increased by means of the Oriel Encoder Mike Controlled Rotation Stage.

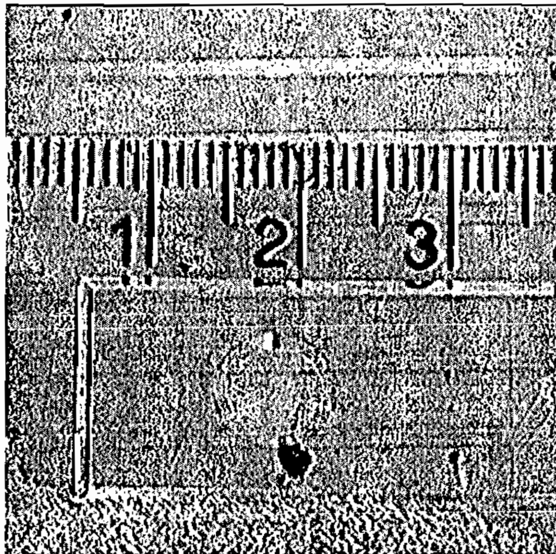

Fig. 4.12 Live image of cylinder with scale

The experimental set-up is exactly as before, with the cylinder taking the place of the cube on the rotation stage. The diameter of the cylinder is 40mm and its circumference 126mm and a 48mm section of this is imaged by the camera as shown in Fig. 4.13.

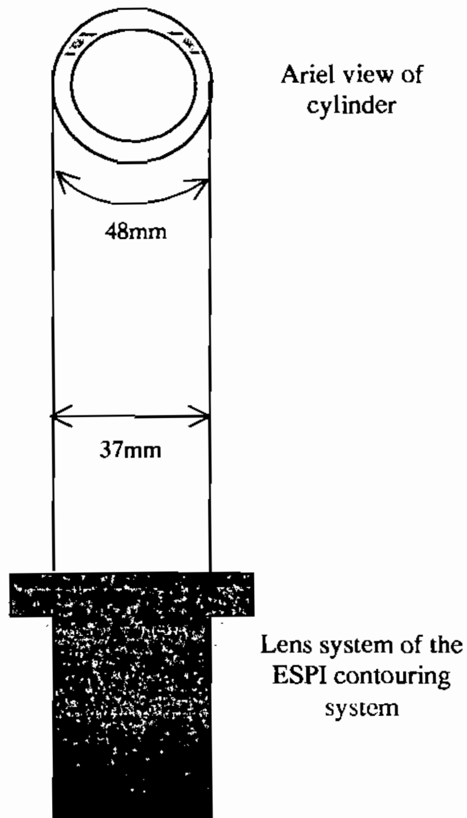

Fig. 4.13 Ariel view of the experimental set-up

The actual values of dϑ for the clockwise experimental series were 0.0062°, 0.01806°, 0.02488°, 0.0311° , 0.0373° and 0.0435°respectively. These angular values correspond to increments of 0.5 of the arbitrary units which the rotation stage uses and are taken for this series of results,. The set of fringe patterns representing the above series is shown in Fig. 4.14 on the following page.

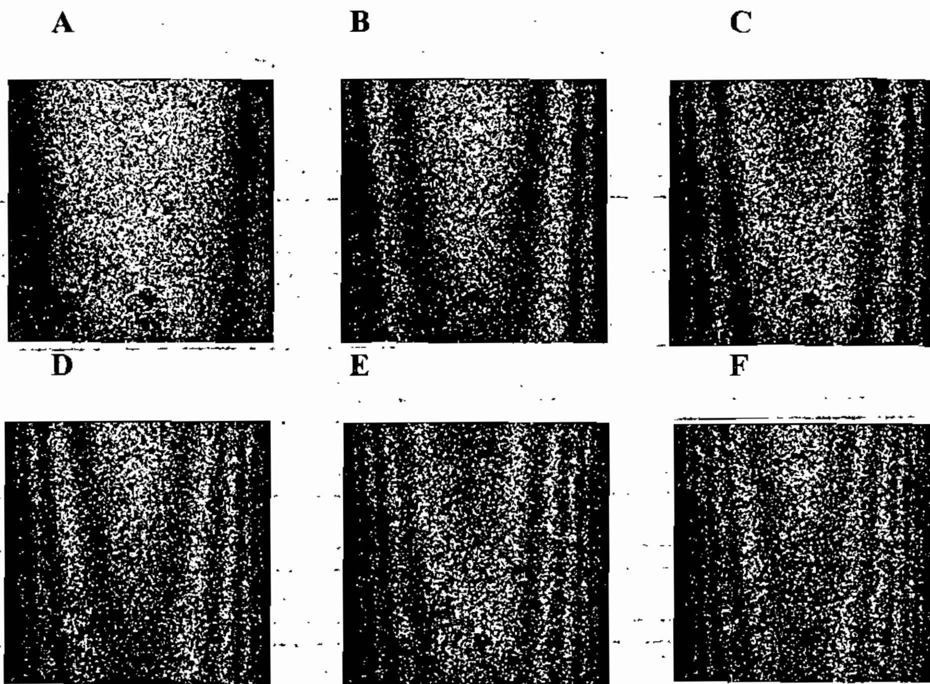

Fig. 4.14 Fringe patterns corresponding to rotations of:. A= 0.0062 °, B= 0.01806 °, C= 0.02488 °, D= 0.0311 °, E= 0.0373 ° and F= 0.0435 °

The fringe contrast diminishes as the fringe number increases. A fringe pattern was chosen with $d\vartheta = 0.0248°$. This gives a Δz value of 3.64mm. The fringe pattern was opened in the image processing package Scion Image as before. Within this package, the millimetre per pixel scale was set and the x-axis positions of the fringes were assigned, see Fig. 4.15. The fringe patterns are slightly assymetrical about the vertical axis, as the plastic pipe used in these experiments was light and hence difficult to secure in a perfectly vertical position and tended to lean backwards somewhat.

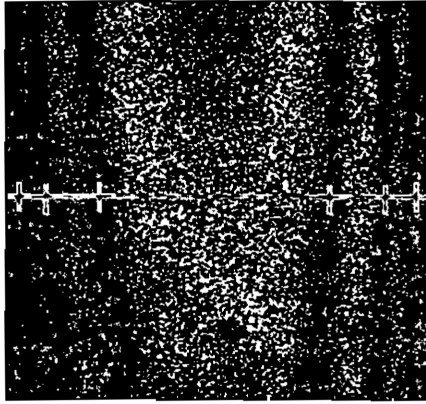

Fig. 4.15 Fringe pattern from cylindrical pipe. . $d\vartheta=0.0248°$

The fringe order was noted and multiplied by the Δz value 3.64mm to give the z-axis values corresponding to the x-axis fringe positions, see Table 4-D:

TABLE 4-D

X-Axis Position/mm	Fringe Order No.	Z-Axis Position/mm
0.67	1	3.64
3.64	2	7.28
8.16	3	10.92
28.65	3	10.92
33.55	2	7.28
36.81	1	3.64

Table 4-D: X- and Z-Axis position / mm with corresponding fringe order number for a cylinder viewed off centre with a clockwise rotation of 0.0248°.

From this tabulated data, it is possible to produce a graph which illustrates the surface profile of the object, by plotting the difference in depth between adjacent fringes, Δz versus the x-axis position of the fringes. This is illustrated in Fig. 4.16.

Fringe Pattern

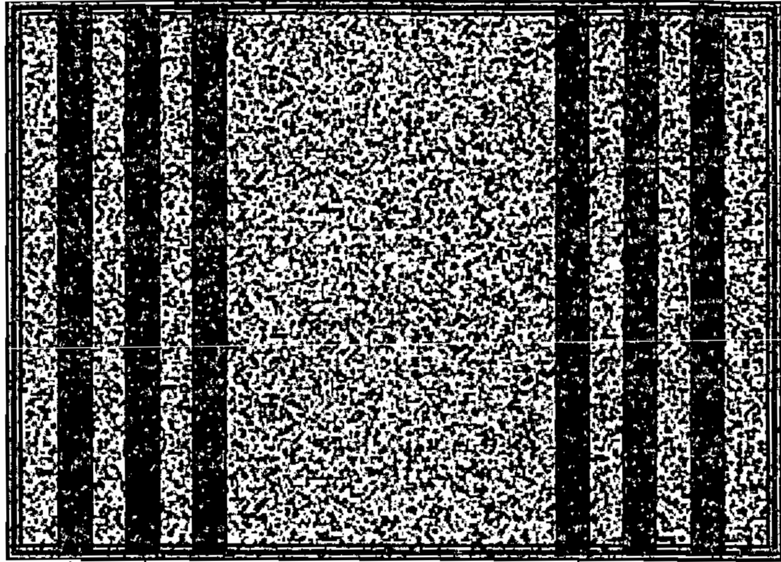

Ariel view of Δz

3-D Cylinder fringe positions

Z-axis Position

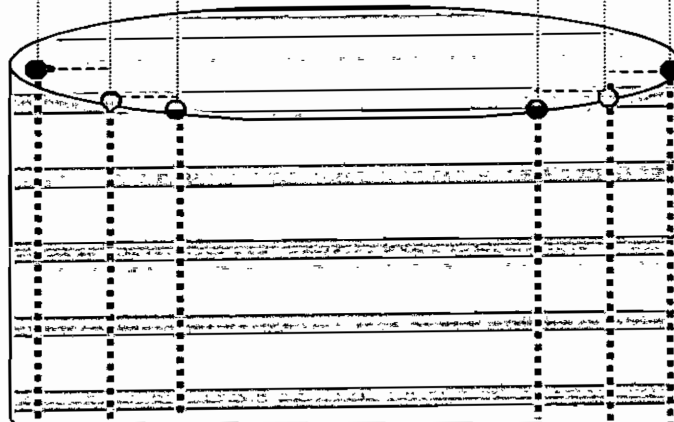

0 X- axis Position 38

Fig. 4.16 Relationship between fringe pattern and object

Plotting the data from Table 4-D, a profile of the cylinder surface is produced See Fig. 4.17.

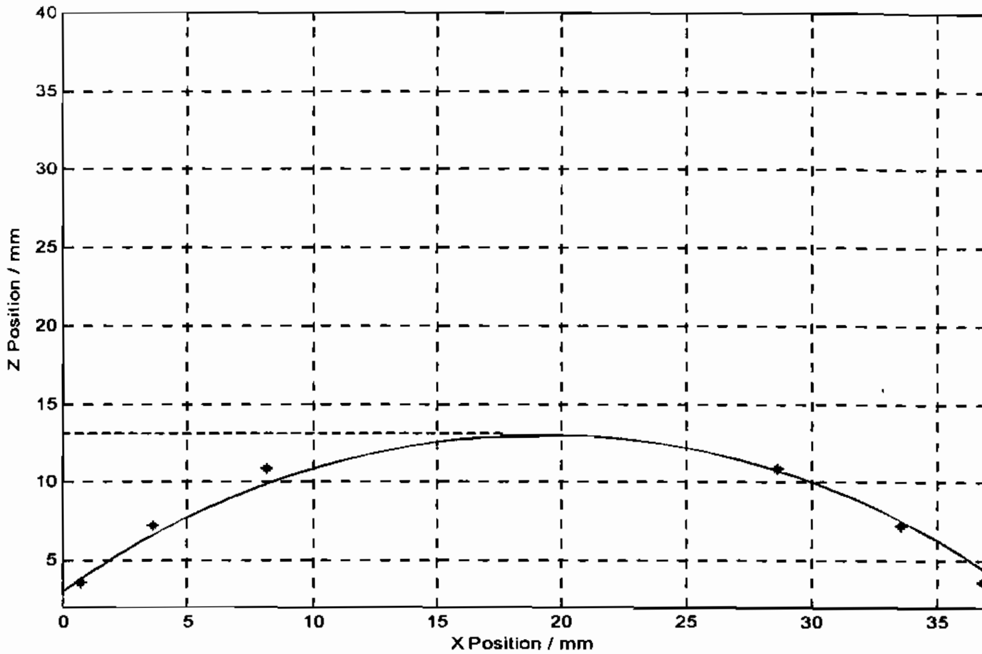

Fig. 4.17 Surface profile of a cylinder

The graph in Fig. 4.17 gives a surface profile which appears to be in agreement with the physical shape of the cylinder being examined. However, in order to prove that the system is effective it is important to read some physical value from this graph and to check its value againest measurements taken from the object. Essentially the graph forms an arc from the circumference of the cylinder with its baseline forming a chord which joins the two points on the circumference which form the arc. This relationship is shown in Fig. 4.18.

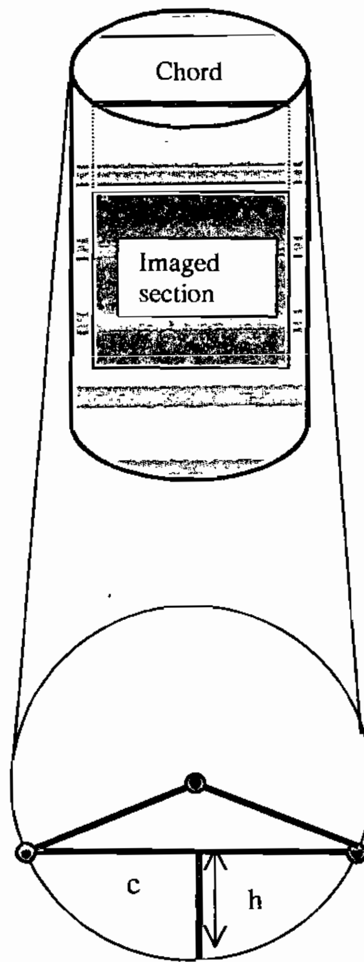

Fig. 4.18 Geometry of the cylinder depth

From Fig. 4.18 , it is clear that there is a relationship between the length of a chord c, and the maximum height h, from the centre of that chord to the circumference. This relationship is easily shown to be[1]

$$h = r - \frac{1}{2}\left(\sqrt{4r^2 - c^2}\right) \qquad 4.1$$

For the cylinder under test in this situation, the radius is 20mm. The chord length is the same as the horizontal area being imaged by the camera, 37mm. Using these measurements, the value for h, the surface height being profiled is 12.4mm. To determine whether or not the system is profiling effectively, the surface height can be read from the graph in Fig. 4.17. By extrapolating from the maximum of the curve to the z-axis, a value of approximately 12.5 mm for the surface height arises. This value, which compares favourably with the geometrically determined value of 12.4mm, shows the system to be an effective and accurate profiler.

It is necessary to analyse another fringe pattern from the same series to demonstrate consistency. A fringe pattern (Fig. 4.19) with 10 fringes and a $d\vartheta$ value of 0.0021° was chosen. Since this fringe pattern was obtained using the same optical set-up as before, the value of ϑ is again 14.4°. The value of Δz for this fringe pattern was found to be 2.1mm.

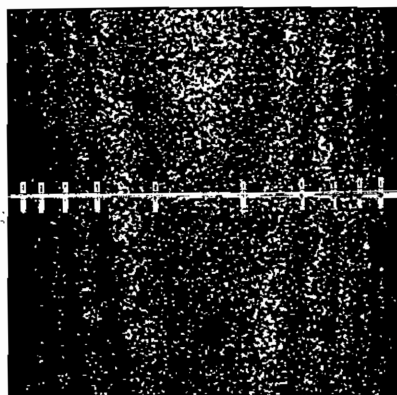

Fig. 4.19 Fringe pattern from cylindrical pipe. $d\vartheta$=0.0436 °

Using the same procedure as before, the necessay data is extracted from the pattern and presented in Table 4-E on the following page.

TABLE 4-E

X-Axis Position/mm	Fringe Order No.	Z-Axis Position/mm
1.56	1	2.1
3.56	2	4.2
5.71	3	6.3
8.54	4	8.4
14.32	5	10.5
23.16	5	10.5
28.72	4	8.4
31.69	3	6.3
33.99	2	4.2
35.70	1	2.1

Table 4-E: X- and Z-Axis position / mm with corresponding fringe order number for a cylinder viewed off centre with a clockwise rotation of 0.0436 °.

Plotting of this quantitative data retrieved from the fringe pattern produces a graph which represents the surface profile of the cylinder as before. See Fig. 4.20.

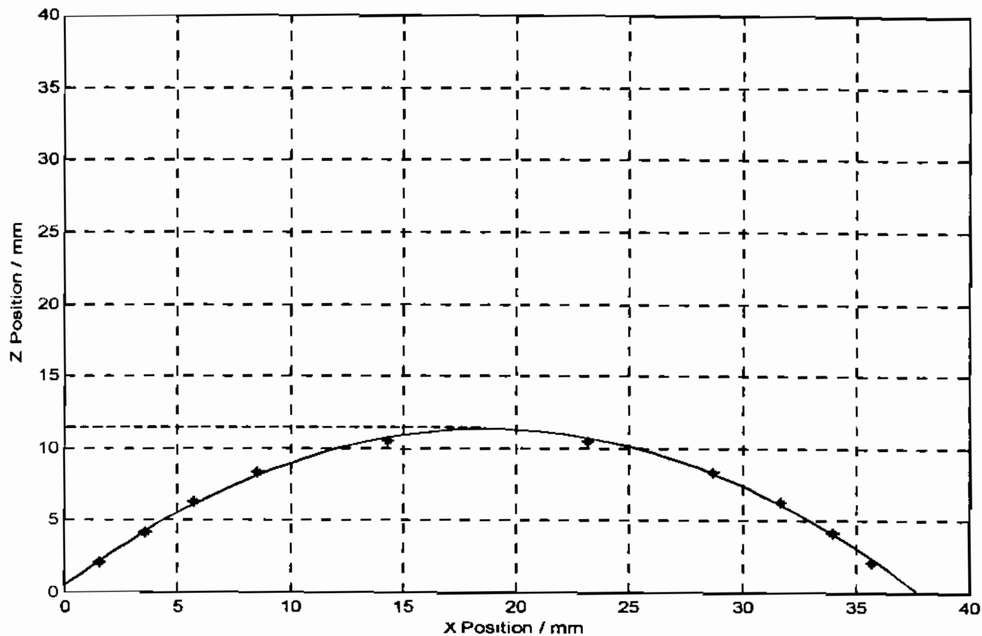

Fig. 4.20 Surface profile of a cylindrical pipe.dϑ=0.0021 °

The surface height is determined from the graph to be approximately 12.2 mm which compares favourably with the known value of 12.4mm.

Through this second series of results, the system has proven to be an effective and accurate method for surface profiling. This section concludes the analysis by fringe counting. In the following chapter, the system is tested again using frequency modulation phase shifting as the method of analysis. The results of these tests are presented.

4.4 References

1. Oberg, E., Jones, F.D., Horton, H.L., "Machinery's Handbook" 21st Edition, Industrial Press Inc., New York, 1980.

5.0 ESPI Results with Phase Shift analysis

5.1 Introduction

As described in earlier chapters, the initial result from an ESPI contouring system is a fringe pattern which maps points of equal surface height. Using the fringe counting method from the previous chapter produced results which show the system to be working effectively. As mentioned in Chapter 2, in the early days of ESPI, before the advent of the phase shifting techniques for analysis, these methods were the only possible way to obtain quantitative data from a fringe pattern.

With the development and decreasing cost of digital image processing equipment, digital fringe analysis techniques have been developed to an extremely high level in recent years. This has been instrumental in the more widespread use of ESPI in both the laboratory and industry due to the fact that it leads to higher accuracy, greater speed and an automated process.

The phase shifting technique has been described in Chapters 2 and 3 along with the algorithm to be used. The technique involves taking one image before rotating the object and 4 images after the object has been rotated with a $\pi/2$ phase shift between these four. The algorithm then works out the change in phase due to the change in the illumination angle. The application of the phase shifting algorithm results in the wrapped phase fringe pattern and this can be unwrapped using an appropriate algorithm.

Too much of a change in illumination angle will lead to decorrelation, as discussed in previous chapters. Indeed, the maximum number of fringes which was achieved before decorrelation during the tests was 8 fringes in most cases. A method to overcome this decorrelation problem is suggested in Chapter 6, "recommendations for further work".

Decorrelation occurs more quickly in this type of ESPI system due to the presence of moving parts. This results in a significant difference in the quality of contrast between this type of system and an in-plane ESPI system for example. The moving part gives rise to a noisy pattern when using the "rotate object" method. While it is possible to produce a phase map and unwrap it using this method, through experiment it has proven to be of poorer contrast than with other ESPI methods. As detailed in Chapter 3, the "rotate beams" method was so unstable in this case as to be incapable of incorporating phase shift analysis due to vibration.

The results presented in this chapter were produced using the "rotate object" method which eliminated the problem with vibration. However, despite the contrast being of high enough quality to enable phase shift analysis, for the most part, the results were affected by noise and resulted in lower quality phase maps, both wrapped and unwrapped. Again, a recommendation has been made in the conclusion regarding these problems.

The Oriel rotation stage has a resolution of 0.0006 ° and so this was the minimum $d\vartheta$ value possible. In general, decorrelation was observed for this experimental set-up after a maximum rotation of 0.0436°. The following experiments were undertaken with the object at a distance of 800mm from the lens, to allow as much of the object surface to be viewed as possible and to allow for more fringes across the object.

5.2 Phase Shift Analysis of a Cube Edge

The cube edge under analysis in Chapter 4, was again the object under test for the first of the "phase -shift analysis" results. As described in the introduction to this chapter, a phase map is produced using the ESPITest software. Such a phase map can be seen in Fig. 5.1 below. The Δz value for this fringe pattern is 7.3 mm.

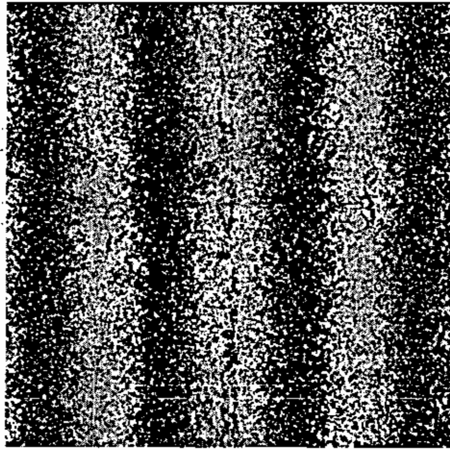

Fig. 5.1 Wrapped phase map corresponding to the surface profile of a cube edge

The software is then used to unwrap this wrapped phase map as mentioned previously. The corresponding unwrapped phase map can be seen in Fig. 5.2.

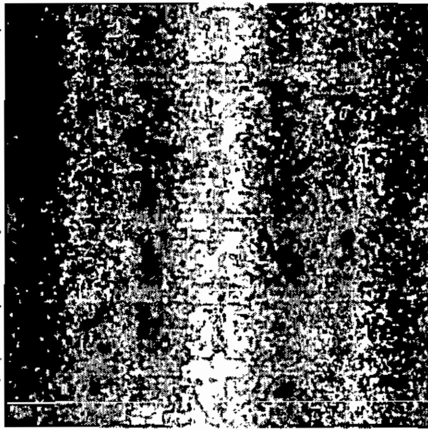

Fig. 5.2 Unwrapped phase map corresponding to Fig. 5.2

The phase map is extremely noisy, displayed as the uneven colour distribution in the grey and white areas. This is due to the continuous movement of the object which is necessary to produce the contour fringes resulting in an averaging of the pixel intensity values. Some median filtering was performed on the data. However, despite this noise, it is clear that surface height information about the cube edge is clearly illustrated in the unwrapped phase map. The white area in the centre corresponds to the edge of the cube, which is closest to the CCD array. The black area at the edges represents the sections of the sides of the cube, which are furthest away while the grey level corresponds to the area in between. Were the data to be less noisy, the grey and white areas would be smoother and blend into one another in a more seamless greyscale, but the basic shape information is there nonetheless.

Fig. 5.3 shows a three-dimensional surface plot, the data for which has been retrieved from the unwrapped phase map.

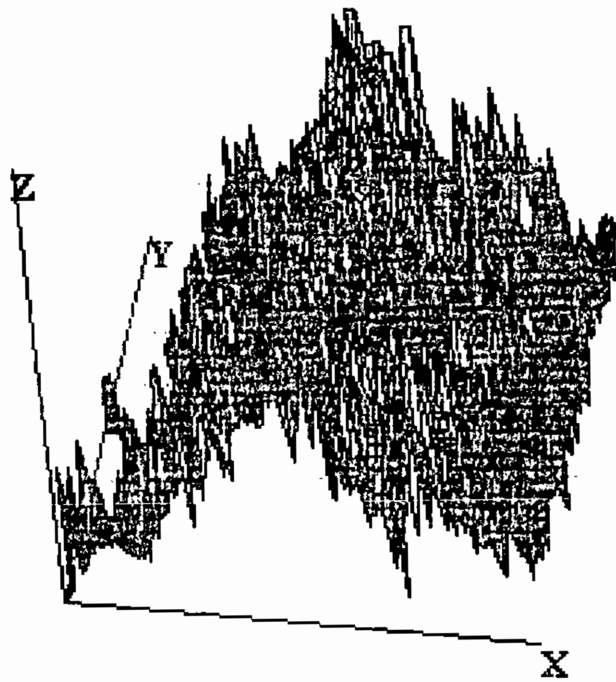

Fig. 5.3 Three-dimensional plot of the cube edge

Despite the presence of considerable noise in the 3-D plot in Fig. 5.3, the basic shape of the cube edge is still clear. The red area in the centre corresponds to the cube edge and the blue regions correspond to the sections of the cube, which were furthest away from the CCD array.

5.3 Phase Shift Analysis of a Pyramid

A pyramid viewed, using the set-up in Fig. 5.4 was then examined using the system.

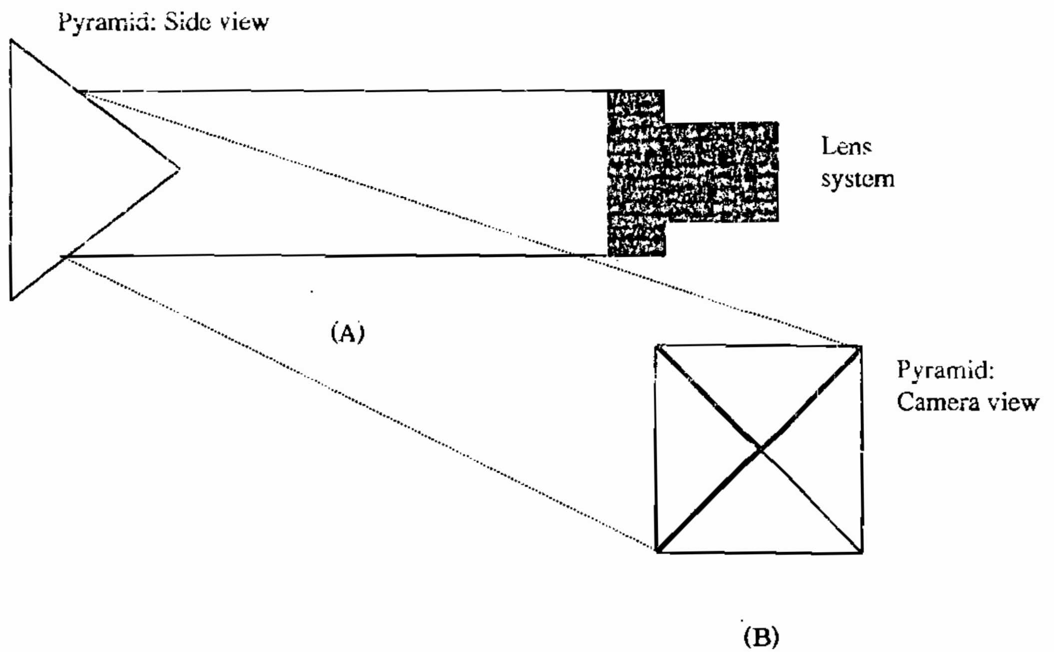

Fig. 5.4 Experimental layout A) Side view B) Camera view of pyramid

As described in the introduction to this chapter, a phase map is produced using the ESPITest software. Such a phase map can be seen in Fig. 5.5. The Δz value for this fringe pattern is 6.6 mm.

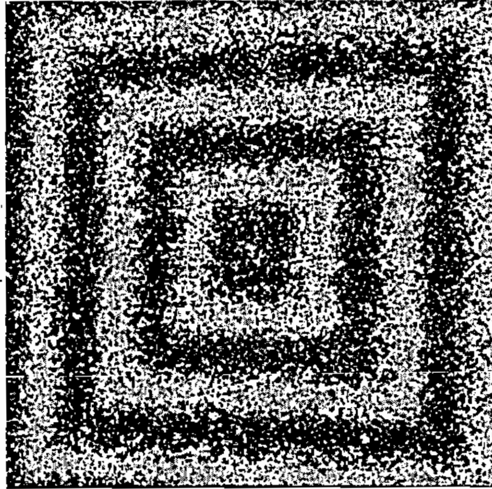

Fig. 5.5 Wrapped phase map of the pyramid

The software is then used to unwrap this wrapped phase map. The corresponding unwrapped phase map can be seen in Fig. 5.6 below.

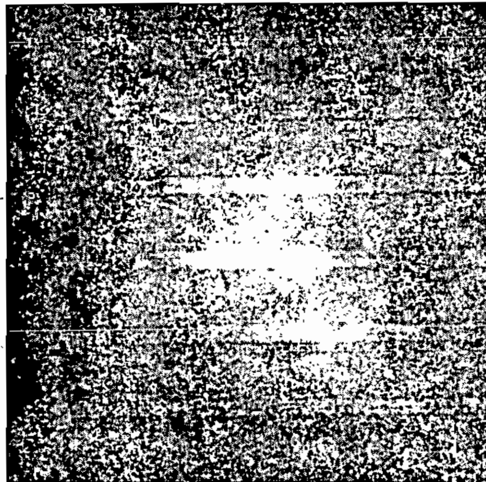

Fig. 5.6 Unwrapped phase map of the pyramid

As before, the bright area in the centre corresponds to the apex of the pyramid which lay closet to the lens in the experimental set-up and hence has the least surface height. The darker area around the edges corresponds to the areas on the pyramid surface, which were furthest away from the viewing system.

Fig. 5.7 illustrates a three dimensional plot using data retrieved from the unwrapped phase map as before.

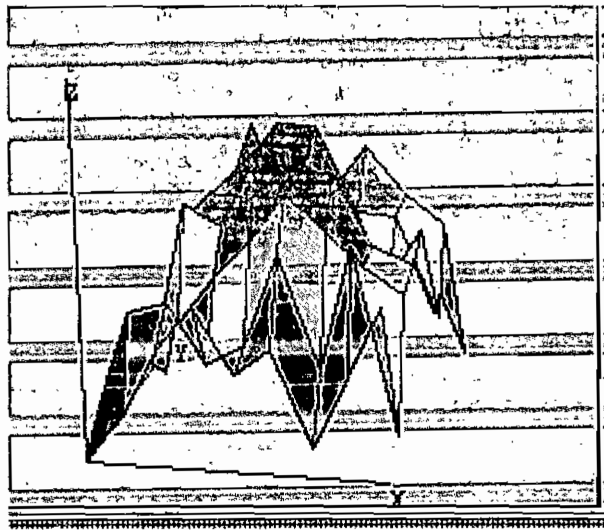

Fig. 5.7 Three dimensional surface plot of the pyramid.

As in the previous example, the noise in the phase map has resulted in a three-dimensional plot with many errors. However, the red region in the centre clearly represents the apex of the pyramid.

5.4 Conclusions

The "rotate object" method has been utilised to produce wrapped phase maps representing the surface profile of the object under test. The software was then used to unwrap these phase maps to produce a greyscale representing surface height. In both cases, this greyscale was converted to a 3D plot of the object.

In each case, the patterns exhibited a great deal of noise due to the movement of the object during operation. With the present system, every effort was made to reduce this effect, however, the final results reflected the movement in the system. The three dimensional plots suggested the basic shape of the object in each case, however, the noise tended to obscure the fine detail of the surface in question. Recommendations to over come this problem have been made in Chapter 6-Conclusions.

Chapter 6.0 Conclusions

6.1 Project conclusions

The ESPI contouring system outlined in the research objectives in Chapter 1 has been produced within the timeframe and budget of the project.

As outlined in the research objectives, it was imperative that the system be miniature, compact and robust, computer controlled, portable and generally suitable for industrial use. Many of the characteristics just mentioned were required in an effort to overcome the reluctance in industry to adopt these techniques.

The system is both miniature and portable, using a laser diode as the light source, miniature optics and measuring 44-cm x 25-cm x 12.5-cm. The duralium beam adds stability to the system making it more robust and enables the system to be mounted on a tripod for portability and industrial use.

The ESPI system is controlled by advanced software, ESPITest which was developed at the Institute for Systems Informatics and Safety laboratories in the European Commission Joint

Research Centre. This user-friendly software acquires the images, subtracts and rectifies the result to produce ESPI fringe patterns which represent the surface profile of an object. It also calibrates and controls the phase shifting device in order to produce wrapped phase maps. These images are then unwrapped by the software. The software also allows filtering of the captured images.

The system provides a whole-field profile of the object under examination, giving it a distinct advantage over some traditional methods for contouring i.e. stylus profilometry. It has been used to produce quantitative results using two different techniques: 1) Fringe counting and 2) phase shifting analysis.

The ESPI contouring system is capable of being used in an industrial environment and the user friendly software means that the user does not necessarily need to be qualified in the particular field of ESPI.

6.2 Recommendations for improvements and further work

Of the two methods for ESPI contouring by angle of illumination change, the "rotate beams" method is the more practically favoured. This is due to the flexibility that the

method allows with the object to be examined. Within the budget constraints of this project, it was not possible to successfully incorporate this method into the system and the "rotate object" method became the method of choice.

The problem of decorrelation with this method could be overcome by using a technique known as phase map addition. Using this technique, the angle of illumination is changed by a small amount, which does not lead to decorrelation, and a phase map produced. The process is repeated and the two resulting wrapped phase maps can be added together to produce a high sensitivity wrapped phase map.

The noise which resulted in reduced quality phase maps occurred due to the movement of the object. Should a suitable budget become available, it is recommended that high quality miniature rotation stages be purchased and incorporated into the system to rotate the beams. This would eliminate the movement of the object and allow the system more flexibility. High quality rotation stages would not exhibit the vibration which the custom made stages did and therefore the contrast should be much improved.

An ideal ESPI contouring system contains no moving parts and so the spectral contouring method described in Chapters 2 and 3 is the most attractive method for shape measurement. It is only a matter of time before high power tunable laser diodes with wavelengths which are compatible with CCD cameras become available so that spectral contouring of large objects can be implemented.

Appendix A- Equipment

1. CCD Camera:

Spindler & Hoyer 930-177 Remote Monochrome CCD Camera
930-535 Wall mounted PSU
512 x 512 pixels

2. Laser:

Make & Model: Ettemeyer laser diode
Wavelength: 785 nm
Max. cw output power: 50 mW
Spectral bandwidth: 2 MHz
Mounting: 9-pin D-sub & cable

3. Laser Current controller:

Make & Model: Ettemeyer LDC 202
Output current range: 0-200mA
Compliance voltage: >6V
Temperature co-efficient: < 50ppm/ ° C
Operation temperature: 0-40 ° C

4. Frame Grabber:

Make & Model: Data Translation DT 3152
Main Features:

- PCI Bus
- Can transfer directly to computer monitor
- 4 monochrome inputs
- Interlaced or non-interlaced
- Programmable gain
- 8-bit resolution
- Pixel Acquisition rate of 20MHz
- One 256 x 8-bit Look up table
- Compatible windows software

5. D/A Board:

Make & Model: National Instruments PC1200/AI
Main Features:

PCI Bus
Two channels
12-bit resolution
1 kS/s update rate
0-10V or ± 5V output
DC output coupling
0.2Ω impedence

6. Custom built Rotation Stage components (From Radionics, Ireland)

440-420 Motor (1.7 deg.) x 2
718-925 Gearbox x 2
718-931 Adapter kit x 2
217-361 Drive System x 2
160-972 33R 50W resistor x 3
158-468 5R 50W resistor x 3
476-075 D Connector x 1
446-478 Plug x 2
446-513 Socket x 2
469-392 Plug shell x 2
469-443 Socket shell x 2
795-937 Heatsink x 4
215-523 Enclosure x 1
597-576 24V 6A Power Supply

7. Oriel Encoder Mike controlled Rotation Stage

Make & Model: Oriel Encoder Mike Controller:

Display resolution 0.1microns
Max speed 200 microns/sec
Min. speed 0.5 microns/sec
Power requirements 110/220-240 VAC 50/60 Hz switch selectable

Mike Specifications

Travel length- 25mm
Angular deviation-

Maximum load-45kg
Angular deviation-22.4 arc sec
Resolution- <0.1 microns
Unidirectional repeatability- <2 microns
Max. speed - 300 microns/sec
Min speed- 0.5 microns/sec

Appendix B- Software

1. ESPITest© written at the European Commission Joint Research Centre, Ispra, Italy

   Windows NT based software package for acquisition, measurement, control and post-processing for electronic speckle pattern interferometry

2. Scion Image

   Base on NIH Image for Macintosh by Wayne Rasband

   National Institutes of Health, U.S.A.

   Modified for Windows by Scion Corporation

   © Scion Corporation 1998, 82, Worman's Mill Court, Suite H, Frederick, Maryland 21703. http://www.scioncorp.com

3. MATLAB © 1984-1999 by The MathWorks, Inc.

   MATLAB is a registered trademark of The MathWorks, Inc.

   Used for all graphing and polynomial fits in Chapter 4.